Table 3 (B) (*continued*)

Genes expressed relatively higher in *Nrf2*$^{+/+}$ mice			Genes expressed relatively higher in *Nrf2*$^{-/-}$ mice		
Name (cluster)[a]	Accession No.	Description	Name (cluster)[a]	Accession No.	Description
Gp1bb (6)	AB001419	Platelet glycoprotein 1b β, PDGF ligand	*Npyr* (2)	Z18280	Neuropeptide hormone receptor NPY-1
Ptp36 (5)	D31842	Protein tyrosine phosphatase	*Fnra* (1)	X79003	Integrin α5 subunit
			Scn71, Nav2.3, Nag (2)	L36179	Voltage-gated sodium channel protein
Transport			Transport		
Nkcc1, Mbsc2 (9)	U13174	Putative basolateral Na-K-2Cl cotransporter	*Cat2* (1)	L03290	Cationic amino acid transporter-2
Nramp (7)	L13732	Integral membrane protein, candidate for Bcg gene	*Pmp34* (2)	AJ006341	Peroxisomal integral membrane protein PMP34
Slc6a6 (4)	AI042802	Similar to Na- and Cl-dependent taurine transporter			
Twik-1 (9)	AF033017	TWIK-1 K^+ channel			
Cd71 (8)	X57349	Transferrin receptor			
Enzymes			Enzymes		
Pkc-α (5)	M25811	Protein kinase Cα	*His, Hsd, Histidase* (1)	L07645	Histidine ammonia-lyase
Tkt, P68 (5)	U05809	Transketolase	*Cpx-1* (1)	AF077738	Metallocarboxypeptidase, similar to CPX-2 and AEBP1
Ldh-2, Ldhb (8)	X51905	Lactate dehydrogenase 2, B chain	*Ly-41, Npps, Pca, Npp1* (1)	J02700	Plasma membrane glycoprotein, ecto-nucleotide phoaphatase
Er-udpase (6)	AJ238636	Nucleoside diphosphatase	*Cf7, FvII* (1)	U66079	Coagulation factor VII, coenzyme A
Pmm2 (6)	AF043514	Phosphomannomutase, SEC53 homolog	*Cpk-m* (1)	U55772	P170 phosphatidyl inositol 3-kinase
Macr1 (6)	U89906	α-Methylacyl-CoA racemase	*Calnc* (3)	M81475	Phosphoprotein phosphatase, calmodulin-dependent
mCask (8)	Y17138	mCASK-B	*C5d* (3)	AB016248	Sterol-C5-desaturase
C62 (8)[b]	U96724	Putative phosphoinositide 5-phosphatase type II			
Dbt (9)	L42996	α-Ketoacid dehydrogenase, mitochondrial			
Pla2g7 (7)	U34277	PAF acetyl hydrolase			
Inflammation and immunity			Inflammation and immunity		
Cathepsin s (9)[b]	AJ223208	Cysteine protease, antigen presentation	*RegIIIγ* (1)	96064	Regenerating gene in islet β-cells, mitogenic
Ly112 (5)[b]	U18424	Bacteria binding macrophage receptor, MARCO	*C10* (1)[c]	M58004	Small inducible cytokine A6
Ccr1,Mip-1a-r (5)	U29678	MIP1-α/Rantes receptor, G-protein coupled	*Vanin 3* (1)	AJ132103	Vanin-3, leukocyte adhesion and homing
Ngp (5)	L37297	Myeloid secondary granule protein	*Scya11* (3)	U77462	Eotaxin, C-C chemokine family
			Evi-1 (3)	M21829	Ecotropic viral integration site1, transcription regulator
			Ltf (1)	J03298	Lactotransferrin precursor, estrogen inducible protein
			Igk-v28 (3)	Z70661	Single chain antibody ScFv
Others			Others		
Aq1 (5)[b]	L02914	Aquaporin-1	*Cx31* (1)[c]	X63099	Connexin 31, gap juction protein
Endomucin (8)[b]	AB034693	Endomucin-1, sialomucin	*Msemk1* (1)	AB017532	msemk1p

Table 3 (B) (*continued*)

Genes expressed relatively higher in $Nrf2^{+/+}$ mice			Genes expressed relatively higher in $Nrf2^{-/-}$ mice		
Name (cluster)[a]	Accession No.	Description	Name (cluster)[a]	Accession No.	Description
Mcl (7)[b]	AF061272	Macrophage-restricted C-type lectin	*Alox12l, 12-Lo* (3)	L34570	12-Lipoxygenase
Creg (9)	AF084524	Cellular repressor of E1A-stimulated gene	*Anx6, Cabm* (2)	X13460	Lipocortin
Phll1 (5)	AB000777	Photolyase/blue-right receptor homolog			

[a] *k*-means clustering subsets in Fig. 2A.
[b] Constitutively overexpressed genes in $Nrf2^{+/+}$ mice relative to $Nrf2^{-/-}$ mice ($p < 0.05$).
[c] Constitutively overexpressed genes in $Nrf2^{-/-}$ mice relative to $Nrf2^{+/+}$ mice ($p < 0.05$).

distinct localization in bronchial basement membrane, endothelium, and alveolar septum.

Discussion

We previously determined NRF2-dependent pulmonary antioxidant/defense enzymes that are potentially important in the protection against pulmonary oxygen toxicity [20]. The present study identified novel genes responsive to oxidative stress and expanded the number of NRF2-regulated genes that could engage, directly or indirectly, in the pathogenesis of oxidative pulmonary injury and protection.

The largest cluster of genes with greater basal and hyperoxia-induced expression in $Nrf2^{+/+}$ mice compared to $Nrf2^{-/-}$ mice contained more than 38 antioxidant/detoxifying enzyme and redox cycle-related protein genes (see Table 3A and Fig. 2D). One of these, thioredoxin reductase (TXNRD), maintains a high ratio of reduced to oxidized thioredoxin, a primary intracellular thiol with redox-buffering capacity similar to that of GSH to reduce H_2O_2 and lipid peroxides [22]. One-Cys peroxiredoxin (CP) belongs to a family of recently recognized antioxidants and is abundant in the lung. CP has GPx and phospholipase A2 activity to protect against lung oxidant injury and phospholipid metabolism [23]. Identification of these antioxidant genes as well as multiple GST isozyme genes, *Glclc*, *Glclr*, *Gpx2*, *Gs-a*, *Gs-b*, and *G6pd*, suggests that a substantial portion of NRF2-mediated pulmonary protection against hyperoxic injury is via cellular defense enzymes associated with thiol metabolism and homeostasis pathways, as depicted in Fig. 6A. Recently, a protective role for a phase 2 defense enzyme (GGT) was functionally determined in hyperoxia models [10,11], which supports the critical antioxidative role of a NRF2–thiol mechanism in oxidative tissue damage. Importantly, we localized NRF2 in the mouse lung. These novel findings indicate that NRF2 is found in airway epithelium and macrophages, where antioxidant enzymes (e.g., GPx2, GSTs) are predominantly expressed. It also further supports functional association of NRF2 and thiol-related antioxidants in protection of the lung from oxidative insult.

Additional NRF2-dependent putative antioxidants in hyperoxic lungs included carboxylesterase (Ex), aldehyde oxidase (AOX)-1, aldehyde dehydrogenases (AHD-2, ALDH3a2, ALDHpb), and ferritin (L subunit). Each has demonstrated antioxidative or detoxifying activity that protects tissues from oxidative stress or injury by various xenobiotics [24–29]. These genes were also recently found to be NRF2-dependent in array analyses with liver models of chemical carcinogenesis [30,31]. Among them, ferritin has a potentially important antioxidant role by sequestering iron to limit its participation in ROS formation, and Tsuji et al. [27] recently identified ARE in the promoter of the ferritin heavy chain. Evidence exists that ferritin protects against hyperoxic lung injury [28] and cellular oxidative stress against xenobiotics [24]. Results of the present study also elucidated several NRF2-dependent cytochrome P450 hydroxylases containing an ARE-like motif (xenobiotic response element) for their transcriptional activation [24]. We found NRF2-dependent non-P450 oxidative enzymes such as alcohol dehydrogenase (ADH-3), AOX-1, and several aldehyde dehydrogenases, some of which bear an ARE motif in their promoters [26].

Novel NRF2-dependent genes upregulated by hyperoxia, but not involved with antioxidant defense, included *Pkc-α*, the major pulmonary PKC isozyme. A protective role for PKC in airways was demonstrated by a genetic linkage analysis in which *Pkc-α* was identified as a candidate protective gene in asthma and pulmonary adenocarcinoma [32]. Importantly, PKC is known to act on the upstream signaling pathway of NRF2 to facilitate its translocation into nuclei. Huang et al. [33] first proposed phosphorylational activation of NRF2 (at Ser40) by PKC. They demonstrated that the Ser40Ala mutation in *Nrf2* led to failure of NRF2 to dissociate from Keap1, a cytosolic inhibitor of NRF2, and inhibited its translocation in response to oxidative stress. This concept has been confirmed by other investigations [34]. Hyperoxia-induced GPx gene expression was dependent on activated PKC in cultured endothelial cells [35]. It is therefore postulated that activation of PKC by hyperoxia induces GPx probably through NRF2 transactivation.

Kinetics of potentially important genes responsive to hyperoxic stress were determined in wild-type ($Nrf2^{+/+}$)

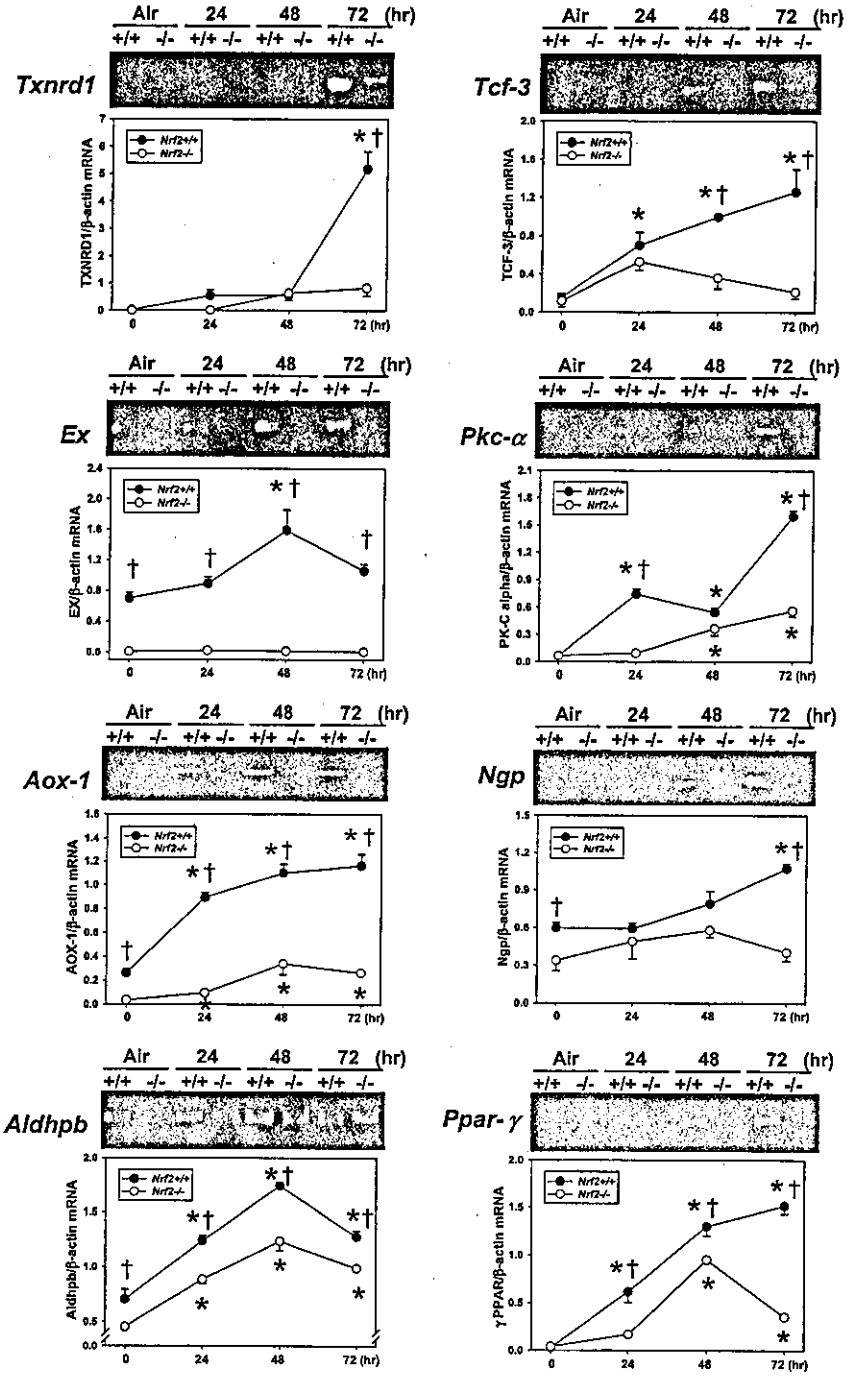

Fig. 3. RT-PCR analyses of representative genes expressed higher in $Nrf2^{+/+}$ mice than in $Nrf2^{-/-}$ mice after hyperoxia exposure. Total lung RNA isolated from the right lung of each mouse (left lung of which was used for array analysis) was processed for RT-PCR analysis to confirm microarray results. Digitized images of cDNA bands on agarose gels were quantitated and normalized to an internal control gene (β-actin) cDNA band. All data are represented as the group means ± SEM (n = 3/group). * Significantly different from genotype-matched air control ($p < 0.05$). †, Significantly different from time-matched $Nrf2^{-/-}$ mice ($p < 0.05$). Representative gel image of each gene is shown above each graph.

animals (see Tables 2A and 2B), and many of the significantly altered genes have not been previously investigated in hyperoxia models. Hyperoxia markedly upregulated numerous genes as early as 24 h before the onset of significant morphological and biological signs of injury (i.e., pulmonary edema, inflammation, septal hyperplasia), and their elevated expression persisted through 48 h or 72 h. Recently, Perkowski et al. [36] determined hyperoxia-responsive genes in the lungs of female C57BL/6J mice at 8–48 h using a Clontech microarray platform. Categories of common genes induced by hyperoxia in their study and the current gene expression profiles of $Nrf2^{+/+}$ mice included genes that encode antioxidants (e.g., GSTs, GPx, HO-1),

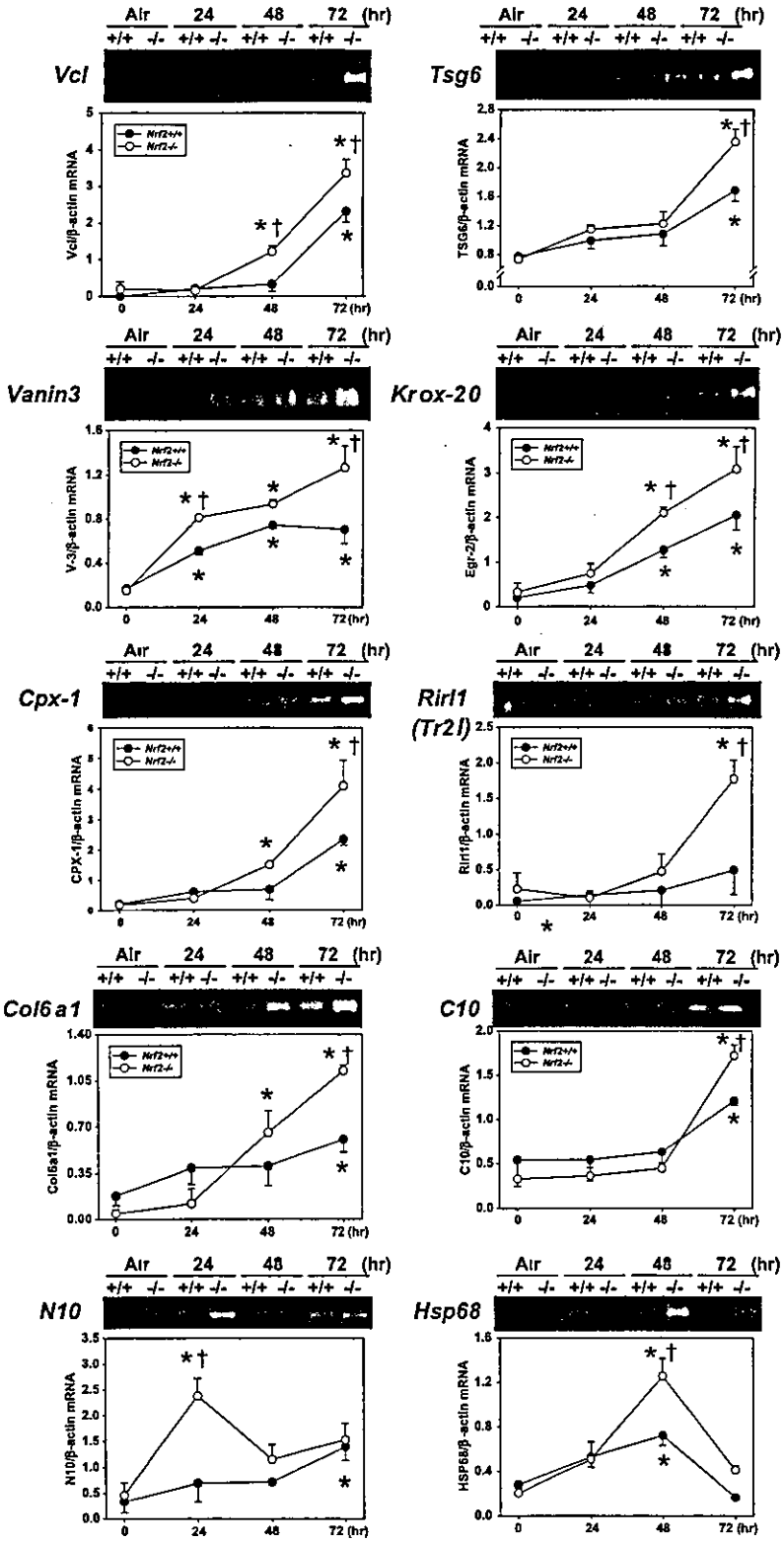

Fig. 4. RT-PCR analyses of representative genes expressed higher in $Nrf2^{-/-}$ mice than in $Nrf2^{+/+}$ mice after hyperoxia exposure. Total lung RNA isolated from the right lung of each mouse, (left lung of which was used for array analysis) was processed for RT-PCR analysis to confirm microarray results. Digitized images of cDNA bands on agarose gels were quantitated and normalized to an internal control gene (β-actin) cDNA band. All data are represented as the group means ± SEM (n = 3/group). * Significantly different from genotype-matched air control ($p < 0.05$). † Significantly different from time-matched $Nrf2^{-/-}$ mice ($p < 0.05$). Representative gel image of each gene is shown above each graph.

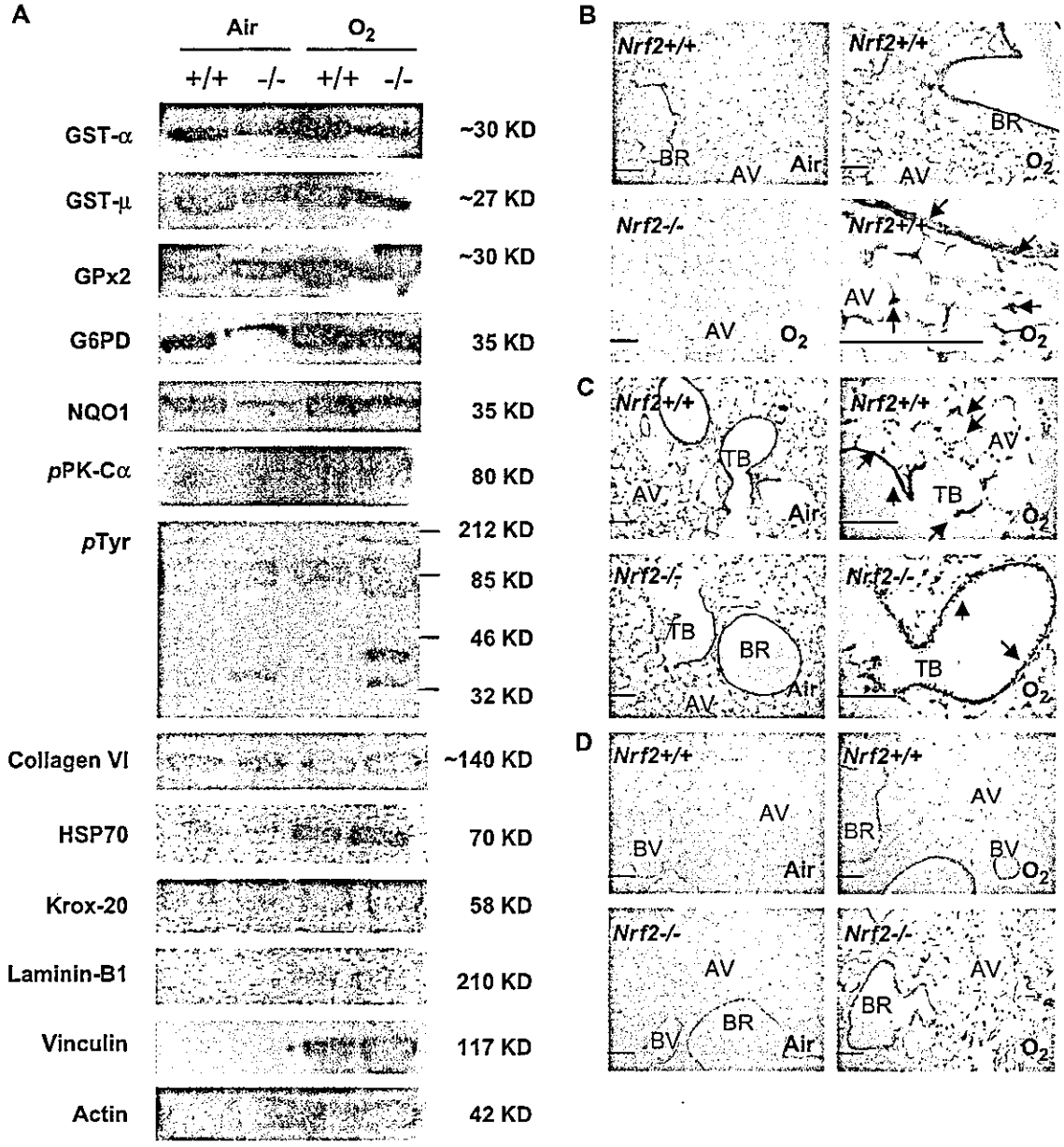

Fig. 5. (A) Differential protein levels of NRF2-dependent genes determined by Western blot analyses. Cytoplasmic and nuclear protein was isolated from right lung homogenates of $Nrf2^{+/+}$ and $Nrf2^{-/-}$ mice exposed to either air or hyperoxia (48 and 72 h), and aliquots were subjected to Western blot analyses using specific antibodies for glutathione *S*-transferase (GST)-α and –μ, glutathione peroxidase(GPx) 2, glucose-6-phosphate dehydrogenase (G6PD), NADP(H):quinone oxidoreductase (NQO) 1, phosphorylated protein kinase C (*p*PKC) α, phosphorylated tyrosine (*p*Tyr), type VI collagen (α1), heat shock protein (HSP) 70, Krox-20 (Egr-2, Zfp-25), laminin-B1, and vinculin. Actin was determined as a constitutive protein control. Representative images from two to four independent analyses of air and peak expression are shown. (B–D) Lung tissue sections were immunohistochemically stained to localize NRF2 [(B) Note high magnification of $Nrf2^{+/+}$ lung section exposed to hyperoxia. Only hyperoxia-exposed lung section presented for $Nrf2^{-/-}$ mice], GPx2 (C), and collagen VI (D) in the lungs from $Nrf2^{+/+}$ and $Nrf2^{-/-}$ mice after air and hyperoxia exposure (72-h data shown). Brown staining indicates antigen deposition. AV, alveoli; BR, bronchiole; TB, terminal bronchiole; BV, blood vessel. Bars indicate 100 μm.

metallothionein, apoptosis genes such as *Bax*, calcium channel genes, and genes related to vascular endothelium. These investigators analyzed data focused on early events (at 24 h) such as apoptosis because hyperoxia-modulated genes were significantly changed mostly at 24 h after hyperoxia in their study. They also demonstrated that more genes were downregulated rather than upregulated at this early time of exposure in these mice. Differences in genes on the array chips or in animals (gender or strain) may account for differences between studies.

Another distinctive gene cluster induced by hyperoxia included extracellular matrix proteins (see Table 2A). In addition to collagens, excessive deposition of microfilaments such as laminins and fibrillins has been considered as an important marker of epithelium-to-mesenchyme

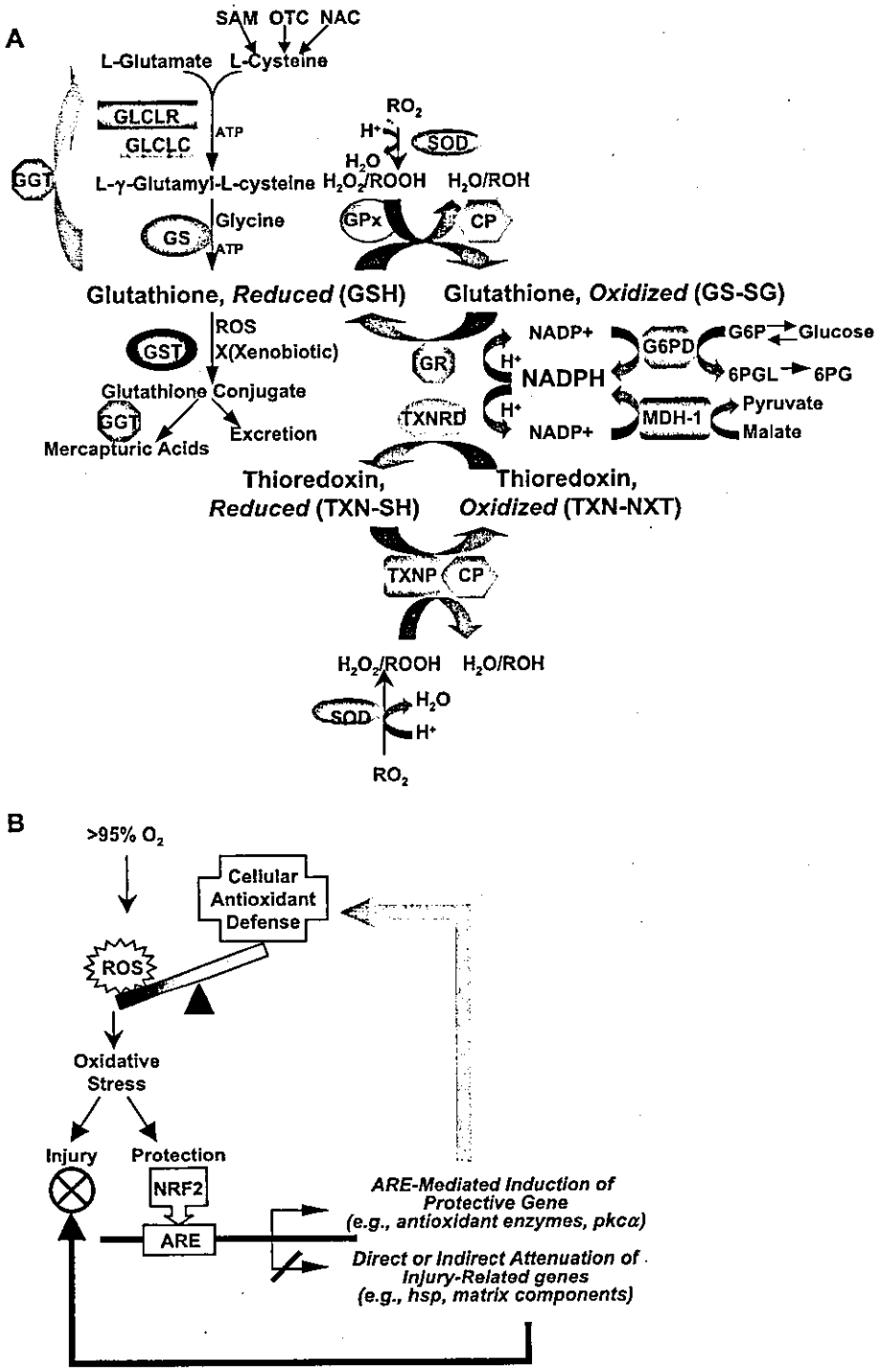

Fig. 6. (A) Proposed primary downstream pathway of NRF2 presents the role of ARE-containing thiol-related antioxidant/redox-cycle enzymes in hyperoxia-injured lungs. SOD, superoxide dismutase; GLCLR, γ-glutamylcysteine ligase regulatory subunit; GLCLC, γ-glutamylcysteine ligase catalytic subunit; GS, glutathione synthetase; GPx, glutathione peroxidase; GR, glutathione reductase; CP, 1-cysteine peroxiredoxin; GST, glutathione *S*-transferase; TXNRD, thioredoxin reductase; TXNP, thioredoxin peroxidase; G6PD, glucose-6-phosphate dehydrogenase; MDH-1, malate dehydrogenase-1; GGT, γ-glutamyl transpeptidase; SAM, *S*-adenosyl-L-methionine; NAC, *N*-acetyl-L-cysteine; OTC, 2-oxothiazolidine-4-carboxylate; 6PGL, 6-phosphogluconolactone; 6PG, 6-phosphogluconate. (B) Putative simplified scheme of hyperoxic injury and protective role of NRF2 in lungs.

transition during airway remodeling [37]. Vinculin, an actin-binding adhesion molecule for cytoskeletal anchoring to the nuclear and cell membrane, is known to increase during the change of cytoskeletal architecture by oxidative stress [38]. Proteolytic activity of various matrix metalloproteinases (MMPs) including MMP9 produced by resident lung cells and various inflammatory cells is also important in pulmonary reepithelialization immediately after acute inhalation injury [39,40]. In addition, the plasminogen system (i.e., plasminogen, urokinase-type

plasminogen activator, tissue-type plasminogen activator in matrix is the primary physiological fibrinolytic pathway through MMP activation [41]. Taken together, marked induction of these genes in the injured lung strongly indicates their coordinated roles in the airway repair and remodeling process after hyperoxia exposure. Importantly, many of these extracellular matrix and cytoskeletal genes were more highly expressed in susceptible $Nrf2^{-/-}$ mice compared to $Nrf2^{+/+}$ mice after exposure (see Table 3B). Some genes were also constitutively higher in $Nrf2^{-/-}$ mice. This suggests that NRF2 is involved in their transcriptional regulation in either normal or oxygen-injured lungs. No evidence exists for the presence of ARE sequences in their promoter. It is therefore postulated that instead of direct modulation of these genes by NRF2, increased oxidative burden by suppression of antioxidant defense mechanisms in $Nrf2^{-/-}$ mice secondarily triggers matrix and structural component genes required for adaptation responses (i.e., repair or reconstitution) against further lung injury (Fig. 6B).

It is well known that hyperoxia causes DNA injury and apoptosis in pulmonary tissues. Many genes involved in apoptosis/survival signals were identified to be hyperoxia inducible in the present analysis (see Table 2A). Among these is *Gadd45* (growth arrest and DNA damage-inducible 45γ), which is regulated through p53 in hyperoxia-injured lungs [42] as well as in many types of cancer cells, including those in the lung [43], to repair DNA fragmentation. Genes encoding heat shock response proteins comprise another cluster that is highly induced by hyperoxia at the early phase of injury. Similar to the extracellular matrix components, early induction of 70-kDa HSP genes (*Hsp68* and *Hsp40*, [44]) was potentiated in the absence of *Nrf2*. This suggests their participation in lung stress responses against hyperoxia as previously indicated [45].

Although our current study focused on genes upregulated by inhaled oxygen, numerous genes and ESTs were downregulated throughout exposure (see Table 2B). Genes such as GTPases, including *Gtpi* (interferon -γ-induced GTPase) may be particularly important because they were differentially suppressed between $Nrf2^{+/+}$ and $Nrf2^{-/-}$ mice. GTP-binding/hydrolyzing proteins induced cell proliferation and hypertrophy via activation of downstream mitogen-activated protein kinase pathways in fibroblasts and endothelial cells after ROS or hyperoxia exposure [22]. *Gtpi* has been shown to induce proliferation of lung cells [46]. Further investigation will be necessary to understand the roles of these downregulated genes in oxidative injury models.

In summary, microarray analysis determined kinetics of hyperoxia-responsive pulmonary genes and identified potentially important NRF2-regulated genes. Newly identified pulmonary antioxidant enzyme/redox-related proteins (e.g., TXNRD1, Ex, CP-2) as well as novel non-antioxidant proteins (e.g., PKC-α, TCF-3, PPARγ) might have key roles in the NRF2-mediated protection against hyperoxic lung injury. Extracellular matrix and structural components as well as heat shock proteins may also have a central role in oxygen-induced airway injury and repair mechanisms. Results from this study provide important insight into molecular mechanisms underlying oxidative lung injury.

Acknowledgments

The National Institute of Environmental Health Sciences, National Institutes of Health, Department of Health and Human Services, and grants (to S.R.) from the National Institutes of Health (ES-03819, ES-09606, HL-073996, HL-66109, HL-57142, NHLBI U01 HL-66614-01, and CA-44530) supported this research. The authors thank Tomohiro Oshimura for his help with the array analyses.

References

[1] Halliwell, B.; Gutteridge, J. M.; Cross, C. E. Free radicals, antioxidants, and human disease: where are we now? *J. Lab. Clin. Med.* **119**:598–620; 1992.

[2] Fahey, J. W.; Talalay, P. Extracellular superoxide dismutase in the airways of transgenic mice reduces inflammation and attenuates lung toxicity following hyperoxia. *Food Chem. Toxicol.* **37**:973–979; 1999.

[3] Itoh, K.; Ishii, T.; Wakabayashi, N.; Yamamoto, M. Regulatory mechanisms of cellular response to oxidative stress. *Free Radic. Res.* **31**:319–324; 1999.

[4] Clerch, L. B. Post-transcriptional regulation of lung antioxidant enzyme gene expression. *Ann. N. Y. Acad. Sci.* **899**:103–111; 2000.

[5] Ho, Y. S.; Dey, M. S.; Crapo, J. D. Antioxidant enzyme expression in rat lungs during hyperoxia. *Am. J. Physiol.* **270**(5 Pt 1):L810–818; 1996.

[6] Crapo, J. D. Morphologic changes in pulmonary oxygen toxicity. *Annu. Rev. Physiol.* **48**:721–731; 1986.

[7] Folz, R. J.; Abushamaa, A. M.; Suliman, H. B. Extracellular superoxide dismutase in the airways of transgenic mice reduces inflammation and attenuates lung toxicity following hyperoxia. *J. Clin. Invest.* **103**:1055–1066; 1999.

[8] Ho, Y. S.; Vincent, R.; Dey, M. S.; Slot, J. W.; Crapo, J. D. Transgenic models for the study of lung antioxidant defense: enhanced manganese-containing superoxide dismutase activity gives partial protection to B6C3 hybrid mice exposed to hyperoxia. *Am. J. Respir. Cell Mol. Biol.* **18**:538–547; 1998.

[9] Tsan, M. F.; White, J. E.; Caska, B.; Epstein, C. J.; Lee, C. Y. Susceptibility of heterozygous MnSOD gene-knockout mice to oxygen toxicity. *Am. J. Respir. Cell Mol. Biol.* **19**:114–120; 1998.

[10] Barrios, R.; Shi, Z. Z.; Kala, S. V.; Wiseman, A. L.; Welty, S. E.; Kala, G.; Bahler, A. A.; Lieberman, M. W. Oxygen-induced pulmonary injury in gamma-glutamyl transpeptidase-deficient mice. *Lung* **179**:319–330; 2001.

[11] Jean, J. C.; Liu, Y.; Brown, L. A.; Marc, R. E.; Klings, E.; Joyce-Brady, M. Gamma-glutamyl transpeptidase deficiency results in lung oxidant stress in normoxia. *Am. J. Physiol. Lung Cell Mol. Physiol.* **283**:L766–776; 2002.

[12] Otterbein, L. E.; Kolls, J. K.; Mantell, L. L.; Cook, J. L.; Alam, J.; Choi, A. M. Exogenous administration of heme oxygenase-1 by

gene transfer provides protection against hyperoxia-induced lung injury. *J. Clin. Invest.* **103**:1047–1054; 1999.

[13] Cho, H. Y.; Jedlicka, A. E.; Reddy, S. P.; Zhang, L. Y.; Kensler, T. W.; Kleeberger, S. R. Linkage analysis of susceptibility to hyperoxia: Nrf2 is a candidate gene. *Am. J. Respir. Cell Mol. Biol.* **26**:42–51; 2002.

[14] Itoh, K.; Chiba, T.; Takahashi, S.; Ishii, T.; Igarashi, K.; Katoh, Y.; Oyake, T.; Hayashi, N.; Satoh, K.; Hatayama, I.; Yamamoto, M.; Nabeshima, Y. An Nrf2/small Maf heterodimer mediates the induction of phase II detoxifying enzyme genes through antioxidant response elements. *Biochem. Biophys. Res. Commun.* **236**:313–322; 1997.

[15] Chan, K.; Kan, Y. W. Nrf2 is essential for protection against acute pulmonary injury in mice. *Proc. Natl. Acad. Sci. USA* **96**: 12731–12736; 1999.

[16] Cho, H. Y.; Reddy, S. P. M.; Yamamoto, M.; Kleeberger, S. R. The transcription factor NRF2 protects against pulmonary fibrosis. *FASEB J.* **18**:1258–1260; 2004.

[17] Ishii, T.; Itoh, K.; Takahashi, S.; Sato, H.; Yanagawa, T.; Katoh, Y.; Bannai, S.; Yamamoto, M. Transcription factor Nrf2 coordinately regulates a group of oxidative stress-inducible genes in macrophages. *J. Biol. Chem.* **275**:16023–16029; 2000.

[18] Shih, A. Y.; Johnson, D. A.; Wong, G.; Kraft, A. D.; Jiang, L.; Erb, H.; Johnson, J. A.; Murphy, T. H. Coordinate regulation of glutathione biosynthesis and release by Nrf2-expressing glia potently protects neurons from oxidative stress. *J. Neurosci.* **23**:3394–3406; 2003.

[19] Venugopal, R.; Jaiswal, A. K. Nrf2 and Nrf1 in association with Jun proteins regulate antioxidant response element-mediated expression and coordinated induction of genes encoding detoxifying enzymes. *Oncogene* **17**:3145–3156; 1998.

[20] Cho, H. Y.; Jedlicka, A. E.; Reddy, S. P.; Kensler, T. W.; Yamamoto, M.; Zhang, L. Y.; Kleeberger, S. R. Role of NRF2 in protection against hyperoxic lung injury in mice. *Am. J. Respir. Cell Mol. Biol.* **26**:175–182; 2002.

[21] Buckley, S.; Driscoll, B.; Barsky, L.; Weinberg, K.; Anderson, K.; Warburton, D. ERK activation protects against DNA damage and apoptosis in hyperoxic rat AEC2. *Am. J. Physiol. Lung Cell Mol. Physiol.* **277**:L159–L166; 1999.

[22] Thannickal, V. J.; Fanburg, B. L. Reactive oxygen species in cell signaling. *Am. J. Physiol. Lung Cell Mol. Physiol.* **279**:L1005–L1028; 2000.

[23] Kim, H. S.; Pak, J. H.; Gonzales, L. W.; Feinstein, S. I.; Fisher, A. B. Regulation of 1-cys peroxiredoxin expression in lung epithelial cells. *Am. J. Respir. Cell Mol. Biol.* **27**:227–233; 2002.

[24] Hayes, J. D.; Ellis, E. M.; Neal, G. E.; Harrison, D. J.; Manson, M. M. Cellular response to cancer chemopreventive agents: contribution of the antioxidant responsive element to the adaptive response to oxidative and chemical stress. *Biochem. Soc. Symp.* **64**:141–168; 1999.

[25] Moorthy, B.; Parker, K. M.; Smith, C. V.; Bend, J. R.; Welty, S. E. Potentiation of oxygen-induced lung injury in rats by the mechanism-based cytochrome P-450 inhibitor, 1-aminobenzotriazole. *J. Pharmacol. Exp. Ther.* **292**:553–560; 2000.

[26] Sreerama, L.; Sladek, N. E. Three different stable human breast adenocarcinoma sublines that overexpress ALDH3A1 and certain other enzymes, apparently as a consequence of constitutively upregulated gene transcription mediated by transactivated EpREs (electrophile responsive elements) present in the 5′-upstream regions of these genes. *Chem.-Biol. Interact.* **130-132**:247–260; 2001.

[27] Tsuji, Y.; Ayaki, H.; Whitman, S. P.; Morrow, C. S.; Torti, S. V.; Torti, F. M. Coordinate transcriptional and translational regulation of ferritin in response to oxidative stress. *Mol. Cell Biol.* **16**:5818–5827; 2000.

[28] Yang, F.; Coalson, J. J.; Bobb, H. H.; Carter, J. D.; Banu, J.; Ghio, A. J. Resistance of hypotransferrinemic mice to hyperoxia-induced lung injury. *Am. J. Physiol. Lung Cell. Mol. Biol.* **277**(6 Pt 1): L1214–1223; 1999.

[29] Zhu, W.; Song, L.; Zhang, H.; Matoney, L.; LeCluyse, E.; Yan, B. Dexamethasone differentially regulates expression of carboxylesterase genes in humans and rats. *Drug Metab. Dispos.* **28**:186–191; 2000.

[30] Kwak, M. K.; Wakabayashi, N.; Itoh, K.; Motohashi, H.; Yamamoto, M.; Kensler, T. W. Modulation of gene expression by cancer chemopreventive dithiolethiones through the Keap1–Nrf2 pathway: identification of novel gene clusters for cell survival. *J. Biol. Chem.* **278**:8135–8145; 2003.

[31] Thimmulappa, R. K.; Mai, K. H.; Srisuma, S.; Kensler, T. W.; Yamamoto, M.; Biswal, S. Identification of Nrf2-regulated genes induced by the chemopreventive agent sulforaphane by oligonucleotide microarray. *Cancer Res.* **62**:5196–5203; 2002.

[32] Dwyer-Nield, L. D.; Paigen, B.; Porter, S. E.; Malkinson, A. M. Quantitative trait locus mapping of genes regulating pulmonary PKC activity and PKC-alpha content. *Am. J. Physiol. Lung Cell Mol. Physiol.* **279**:L326–332; 2000.

[33] Huang, H. C.; Nguyen, T.; Pickett, C. B. Phosphorylation of Nrf2 at Ser-40 by protein kinase C regulates antioxidant response element-mediated transcription. *J. Biol. Chem.* **277**:42769–42774; 2002.

[34] Hess, A.; Wijayanti, N.; Pathe Neuschafer-Rube, A.; Katz, N.; Kietzmann, T.; Immenschuh, S. Phorbol ester-dependent activation of peroxiredoxin I gene expression via a protein kinase C, Ras, p38 mitogen-activated protein kinase signaling pathway. *J. Biol. Chem.* **278**:45419–45434; 2003.

[35] Jornot, L.; Junod, A. F. Hyperoxia, unlike phorbol ester, induces glutathione peroxidase through a protein kinase C-independent mechanism. *Biochem. J.* **329**:117–123; 1997.

[36] Perkowski, S.; Sun, J.; Singhal, S.; Santiago, J.; Leikauf, G. D.; Albelda, S. M. Gene expression profiling of the early pulmonary response to hyperoxia in mice. *Am. J. Respir. Cell Mol. Biol.* **28**: 682–696; 2003.

[37] Rosenbloom, J.; Abrams, W. R.; Mecham, R. Extracellular matrix 4: the elastic fiber. *FASEB J.* **7**:1208–1218; 1993.

[38] Malorni, W.; Iosi, F.; Mirabelli, F.; Bellomo, G. Cytoskeleton as a target in menadione-induced oxidative stress in cultured mammalian cells: alterations underlying surface bleb formation. *Chem.-Biol. Interact.* **80**:217–236; 1991.

[39] Legrand, C.; Gilles, C.; Zahm, J. M.; Polette, M.; Buisson, A. C.; Kaplan, H.; Birembaut, P.; Tournier, J. M. Airway epithelial cell migration dynamics; MMP-9 role in cell–extracellular matrix remodeling. *J. Cell Biol.* **146**:517–529; 1999.

[40] Vu, T. H.; Werb, Z. Matrix metalloproteinases: effectors of development and normal physiology. *Genes Dev.* **14**:2123–2133; 2000.

[41] Lijnen, H. R. Elements of the fibrinolytic system. *Ann. N. Y. Acad. Sci.* **936**:226–236; 2001.

[42] O'Reilly, M. A.; Staversky, R. J.; Watkins, R. H.; Maniscalco, W. M.; Keng, P. C. p53-independent induction of GADD45 and GADD153 in mouse lungs exposed to hyperoxia. *Am. J. Physiol. Lung Cell Mol. Physiol.* **278**:L552–559; 2000.

[43] Tchou-Wong, K. M.; Jiang, Y.; Yee, H.; LaRosa, J.; Lee, T. C.; Pellicer, A.; Jagirdar, J.; Gordon, T.; Goldberg, J. D.; Rom, W. N. Lung-specific expression of dominant-negative mutant p53 in transgenic mice increases spontaneous and benzo(a)pyrene-induced lung cancer. *Am. J. Respir. Cell Mol. Biol.* **27**:186–193; 2002.

[44] Hernandez, M. P.; Sullivan, W. P.; Toft, D. O. The assembly and intermolecular properties of the hsp70–Hop–hsp90 molecular chaperone complex. *J. Biol. Chem.* **277**:38294–38304; 2002.

[45] Wong, H. R.; Menendez, I. Y.; Ryan, M. A.; Denenberg, A. G.; Wispe, J. R. Increased expression of heat shock protein-70 protects A549 cells against hyperoxia. *Am. J. Physiol. Lung Cell. Biol.* **275**(4 Pt 1): L836–841; 1998.

[46] Gorbacheva, V. Y.; Lindner, D.; Sen, G. C.; Vestal, D. J. The interferon (IFN)-induced GTPase, mGBP-2: role in IFN-gamma-induced murine fibroblast proliferation. *J. Biol. Chem.* **277**:6080–6087; 2002.

THE JOURNAL OF BIOLOGICAL CHEMISTRY
Vol. 280, No. 6, Issue of February 11, pp. 4483–4490, 2005
Printed in U.S.A.

Nrf2 Transcriptionally Activates the *mafG* Gene through an Antioxidant Response Element*

Received for publication, October 7, 2004, and in revised form, November 15, 2004
Published, JBC Papers in Press, December 1, 2004, DOI 10.1074/jbc.M411451200

Fumiki Katsuoka‡§¶, Hozumi Motohashi‡§‖, James Douglas Engel, and Masayuki Yamamoto‡§‡‡§§**

*From the ‡Graduate School of Comprehensive Human Sciences, §Center for Tsukuba Advanced Research Alliance, and ‡‡ERATO Environmental Response Project, University of Tsukuba, Tsukuba 305-8577, Japan, and **Department of Cell and Developmental Biology and Center for Organogenesis, University of Michigan, Ann Arbor, Michigan 48109-0616*

Nrf2 accumulates in nuclei upon exposure to oxidative stress, heterodimerizes with a small Maf protein, and activates the transcription of stress target genes through antioxidant response elements (AREs). We found that diethyl maleate (DEM), a well known activator of Nrf2, induces one of the small Maf genes, *mafG*. To elucidate roles MafG might play in the oxidative stress response, we examined transcriptional regulation of the mouse *mafG* gene. *MafG* utilizes three independent first exons that are each spliced to second and third coding exons. Among the small *maf* genes, *mafG* showed the strongest response to DEM, and of the three first exons, the highest -fold induction was seen with the proximal first exon (Ic). Importantly, one ARE (Ic-ARE) is conserved in the promoter flanking exon Ic of the human and mouse *mafG* genes. The Nrf2/MafG heterodimer bound the Ic-ARE and activated transcription, whereas DEM failed to activate *mafG* in *nrf2*-null mutant cells. Chromatin immunoprecipitation further revealed that both Nrf2 and small Maf proteins associate with the Ic-ARE *in vivo*. These results demonstrate that *mafG* is itself an ARE-dependent gene that is regulated by an Nrf2/small Maf heterodimer and suggest the presence of an autoregulatory feedback pathway for *mafG* transcriptional regulation.

Cells have the ability to adapt to oxidative stress or to exposure to xenobiotics. By inducing a battery of antioxidant and xenobiotic metabolizing enzymes, such as glutathione *S*-transferase, heme oxygenase-1 (HO-1),[1] and NAD(P)H:quinone oxidoreductase 1 (NQO1), cells protect themselves from oxidative stress and xenobiotics (1, 2). It has long been known that the genes encoding these enzymes are often coordinately regulated through AREs in their gene-regulatory regions (2). The ARE is a Maf (musculo-aponeurotic fibrosarcoma) recognition element (MARE)-related sequence, with strong similarity to the MARE (3) (see Fig. 4*A*). Basic region-leucine zipper transcription factors, including CNC (Cap'n'Collar protein) family (Nrf1, Nrf2, Nrf3, and p45 NF-E2) and Bach (BTB and CNC homology) proteins (Bach1 and Bach2), form heterodimeric partners with a small Maf protein (MafG, MafK, and MafF), and then associate with various MARE-related sequences (including AREs).

CNC and Bach proteins possess transcriptional activation and repression domains, respectively. Therefore, ARE-mediated transcription is either positively or negatively regulated, depending on which basic region-leucine zipper factors bind to the ARE(s). Whereas small Maf proteins lack any recognizable transcriptional effector domains (other than the basic region-leucine zipper motif), they are nonetheless regarded as critical regulators of ARE-mediated transcription, since CNC and Bach proteins require them as obligatory partners for site-specific association with the ARE. Moreover, it is well documented that homodimers and heterodimers composed exclusively of small Maf proteins can act as repressive competitors to small Maf/CNC and small Maf/Bach heterodimers. One implication of these data is that small Maf proteins can participate in both positive and negative regulation of MARE-dependent genes. Additionally, the amount of small Maf proteins could be an important determinant of the transcriptional activity of target genes (for reviews, see Refs. 4 and 5).

The positive contributions of CNC proteins and the negative contributions of Bach1 to ARE-mediated transcription have been validated by gene targeting strategies. ARE-dependent gene induction was greatly impaired in *nrf2*-null mutant mice (6), and Nrf1 is also reported to contribute to the activation of ARE-dependent genes (7, 8). The ARE-dependent *HO-1* gene was significantly derepressed in *bach1*-null mutant mice, suggesting that *HO-1* is negatively regulated by Bach1 (9). Although *nrf3*-null and *bach2*-null mutant mice have been reported (10, 11), the contribution of these factors to ARE-mediated regulation is still to be determined.

In comparison with the *cnc* and *bach* family-targeted mutant mice, the phenotypes of small *maf* mutant mice were expected to be more complicated, since small Maf proteins can participate in both positive and negative regulation. The functions of small Maf proteins are compensatory and provide partially overlapping redundancy, since small *maf* single mutant mice ($mafG^{-/-}$, $mafK^{-/-}$, and $mafF^{-/-}$) showed mild or subtle phenotypes (12–14), whereas small *maf* compound mutant mice ($mafG^{-/-}$:$mafF^{-/-}$ and $mafG^{-/-}$:$mafF^{-/-}$:$mafK^{-/-}$) displayed a greater number of and more profound deficiencies (15, 16).

* This work was supported by National Institutes of Health Grants CA80088 and GM28896 (to F. K., H. M., and J. D. E.), ERATO-JST (to M. Y.), the Ministry of Education, Science, Sports, and Culture (to H. M. and M. Y.), the Ministry of Health, Labor, and Welfare (to H. M. and M. Y.), CREST (to H. M.), the Atherosclerosis Foundation (to M. Y.), the Naito Foundation (to M. Y.), and the Special Coordination Fund for Promoting Science and Technology (to H. M.). The costs of publication of this article were defrayed in part by the payment of page charges. This article must therefore be hereby marked "*advertisement*" in accordance with 18 U.S.C. Section 1734 solely to indicate this fact.

¶ A Japan Society for the Promotion of Science Research Fellow.
‖ To whom correspondence may be addressed. Tel.: 81-29-853-7320; Fax: 81-29-853-7318; E-mail: hozumim@tara.tsukuba.ac.jp.
§§ To whom correspondence may be addressed. Tel.: 81-29-853-7320; Fax: 81-29-853-7318; E-mail: masi@tara.tsukuba.ac.jp.

[1] The abbreviations used are: HO-1, heme oxygenase-1; ARE, antioxidant response element; ChIP, chromatin immunoprecipitation; DEM, diethyl maleate; EMSA, electrophoretic mobility shift assay; LDH, lactose dehydrogenase; MARE, maf recognition element; MEF, mouse embryonic fibroblast; NQO1, NAD(P)H:quinone oxidoreductase 1; PRDX1, peroxiredoxin 1; RACE, rapid amplification of cDNA ends; RT, reverse transcription.

TABLE I
Oligonucleotide primers and TaqMan probe (see "Experimental Procedures")
FAM, reporter fluorescent dye; TAMRA, quencher fluorecent dye.

Name of oligonucleotide	5′ to 3′ sequence
MafG-Ia	CCGCAGGTTTCTCCCGGGGTGGAAG
MafG-Ib	CAGCCGGATTGCCTGCTACCTGGAAG
MafG-Ic	TTCTGAAGCAGCCAAGCTCAGAGTG
MafG-int	TCCTGACCTATGCTCTGTGTCTT
MafG-III-II	CCTGGCTCCCGCTTCACCTTTAAG
MafG-P (TaqMan probe)	FAM-ACTGTGTCCCCCGGGTTATGACG-TAMRA

We recently observed that a fraction of ARE-dependent genes (*e.g. NQO1* and thioredoxin reductase 1) are not normally induced in either small *maf* compound mutant mice or in *nrf2*-null mutant mice.[2] Therefore, we concluded that small Maf proteins act cooperatively with Nrf2 to activate the transcription of these genes. In contrast, *HO-1* transcription is derepressed in small *maf* compound mutant mice, similarly to the *bach1*-null mutant (16), suggesting that small Maf proteins are also important for collaboratively repressing *HO-1*. In this way, we genetically confirmed that small Maf proteins act as required cofactors in both positive and negative MARE-dependent regulation of gene transcription.

In the course of previous gene expression analyses, we found that diethyl maleate (DEM), a well known inducer of Nrf2/ARE-dependent genes, induced the expression of *mafG*.[3] This observation suggested that *mafG* is an Nrf2/ARE-dependent gene. However, the mechanisms that regulate *mafG* transcription are only poorly understood. Here, we show that a functional promoter ARE controls *mafG* induction. By electrophoretic mobility shift assay (EMSA) and chromatin immunoprecipitation (ChIP) analyses, we demonstrate that Nrf2 and small Maf proteins bind specifically to the *mafG* ARE. We also confirm that induction of *mafG* is severely impaired in *nrf2*-null mutant cells. Thus, *mafG* is indeed an Nrf2/ARE-dependent gene.

EXPERIMENTAL PROCEDURES

Animals—Germ line mutagenesis of mouse *nrf2* was described previously (6). The mice used in this study were on a mixed genetic background of 129SvJ and ICR.

Mouse Embryonic Fibroblasts (MEF)—MEFs were prepared from individual embryos at embryonic day 13.5. The head and internal organs were removed, and the torso was minced and dispersed in 0.25% trypsin/EDTA. MEFs were maintained in Dulbecco's modified Eagle's medium (Sigma) containing 10% fetal bovine serum and antibiotics. To induce ARE-dependent genes, MEFs were treated with 50 μM DEM (Wako Pure Chemicals, Osaka, Japan) for 12 h.

Quantitative RT-PCR—Total RNA was prepared from mouse liver or from mouse embryonic fibroblasts using Isogen (Nippon Gene, Japan) following the recommended protocol. Random cDNA was synthesized from the isolated RNAs, and real time PCR (ABI PRISM 7700) was performed as described (14). Sequences of the primers and probes used for detecting total mafG transcript have been described previously (14), and those used for detecting each mafG transcript are shown in Table I. The mafG-III-II primers and mafG-P TaqMan probe were designed at a region common to all four transcripts.

RNA Blot Analysis—Total RNA was electrophoresed on formaldehyde-agarose gels and transferred to a nylon membrane (Zeta probe; Promega). ^{32}P-Labeled probes were prepared from the cDNAs by random primer labeling. References for the sequences of the cDNAs used in this study are as follows: *HO-1* (17), *NQO1* (6), and peroxiredoxin 1 (*PRDX1*) (17).

Rapid Amplification of cDNA Ends (RACE)—RACE was performed with total RNA from a mouse embryonic day 16.5 embryo utilizing the Marathon cDNA amplification kit according to the manufacturer's instructions (Clontech). The sequences of the gene-specific primers are as follows: MafG-GSP1, 5′-TCA GCT GGA TGA TCT CTT CCT TGG AGA G-3′ and MafG-nested-GSP2, 5′-ACA TGG TTA CCA GCT CCT CGT CGG TCA A-3′. RACE products were subcloned into pGEM-T (Promega), and their sequences were determined.

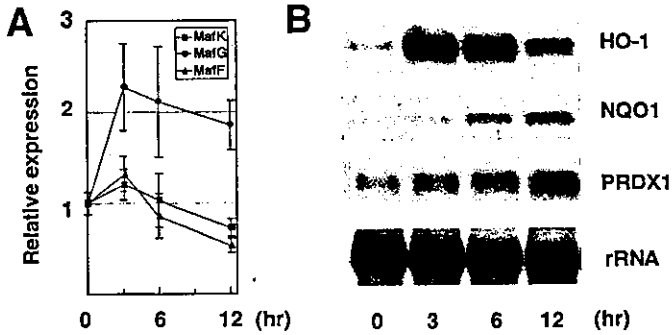

FIG. 1. **DEM induces *mafG* and other ARE-dependent genes.** MEF's of wild type mice were treated with DEM for 0, 3, 6, and 12 h. *A*, quantitative RT-PCR was performed to examine the expressions of MafG, MafK, and MafF mRNAs. The expression of each small *maf* gene at 0 h was set to 1. The *error bars* represent the S.D. values ($n = 3$). *B*, RNA blot analysis was performed to examine the expressions of *HO-1*, *NQO1*, and *PRDX1* genes. rRNA was used as a loading control.

Electrophoretic Mobility Shift Assay (EMSA)—Nrf2CT (18) and MafG 1–123 (19) were tagged with 6 histidine residues at the N termini and purified by nickel chelation affinity chromatography. The oligonucleotides NQO1-ARE-F (5′-CGC GTC TGA ACT TTC AGT CTA GAG TCA CAG TGA GTC GGC AAA ATT-3′) and MafG-ARE-F (5′-CGC GCG ATC CGC TGA GTC AGC ATG ACT CGC CAG GAA CAG GGC GCT-3′) were radiolabeled with ^{32}P and annealed with the complementary strand oligonucleotides NQO1-ARE-R (5′-CTA GAA ATT TTG CCG ACT CAC TGT GAC TCT AGA CTG AAA GTT CAG A-3′) and MafG-ARE-R (5′-CTA GAG CGC CCT GTT CCT GGC GAG TCA TGC TGA CTC AGC GGA TCG-3′), respectively. To generate unlabeled competitors, a pair of oligonucleotides MafG-ARE-F and MafG-ARE-R (above; wild type competitor) and their corresponding mutant oligonucleotides with base substitutions shown in Fig. 5*C* (m1, m2, and m3 competitors) were annealed. An increasing amount of competitors, from 10- to 100-fold or a 300-fold excess of competitors was added. Incubation of the probe and recombinant proteins with or without unlabeled competitors was carried out as described previously (3). The protein-DNA complexes and free probe were resolved by electrophoresis on a 5% polyacrylamide (79:1) gel in 1× TBE buffer.

Transfection—293T cells were maintained in Dulbecco's modified Eagle's medium containing 10% fetal bovine serum and antibiotics and seeded in a 12-well plate 24 h before transfection. Mouse Nrf2 cDNA was inserted into pEF-BssHII (3) and used for transient expression of Nrf2 (pEF-Nrf2). pIM-MafG (20) was used for transient expression of mouse MafG. To make pNQO1-ARE-Luc, the pair of oligonucleotides NQO1-ARE-F and NQO1-ARE-R (above) were annealed and inserted into pRBGP3 (21). To generate pMafG-ARE-Luc and their mutant derivatives, a pair of oligonucleotides MafG-ARE-F and MafG-ARE-R (above), either bearing or without any introduced mutation (Fig. 5*C*), were annealed and inserted into pRBGP3. These expression vectors and the luciferase reporter vectors were transfected into the cells using FuGENE6 (Roche Applied Science). 12 h after transfection, cells were harvested, and the lysates were used for luciferase assays. The expressions of both firefly and sea pansy luciferase were quantified using a dual luciferase reporter assay (Promega); firefly luciferase activity was normalized to co-transfected sea pansy luciferase activity for transfection efficiency.

ChIP Analysis—ChIP analysis was performed essentially as described previously (22). Immunoprecipitations were performed using control rabbit IgG, anti-Nrf2, or anti-p18/MafK antibodies (Santa Cruz Biotechnology, Inc., Santa Cruz, CA). Immunoprecipitated material or a 1:50 dilution of input was used for PCR with the following primers: *NQO1* ARE (22); lactate dehydrogenase (LDH) gene promoter (22); and *mafG* Ic promoter, (5′-GGC TGA TCC TTG CTT GCT GTT G-3′ and 5′-GCA AGC CTA GAA GGA AGC TGA G-3′).

RESULTS

MafG Gene Expression Is Induced by DEM—In an earlier study, we found that DEM, a well known inducer of Nrf2/ARE-

[2] F. Katsuoka, H. Motohashi, J. D. Engel, and M. Yamamoto, unpublished observations.
[3] F. Katsuoka, H. Motohashi, J. D. Engel, and M. Yamamoto, submitted for publication.

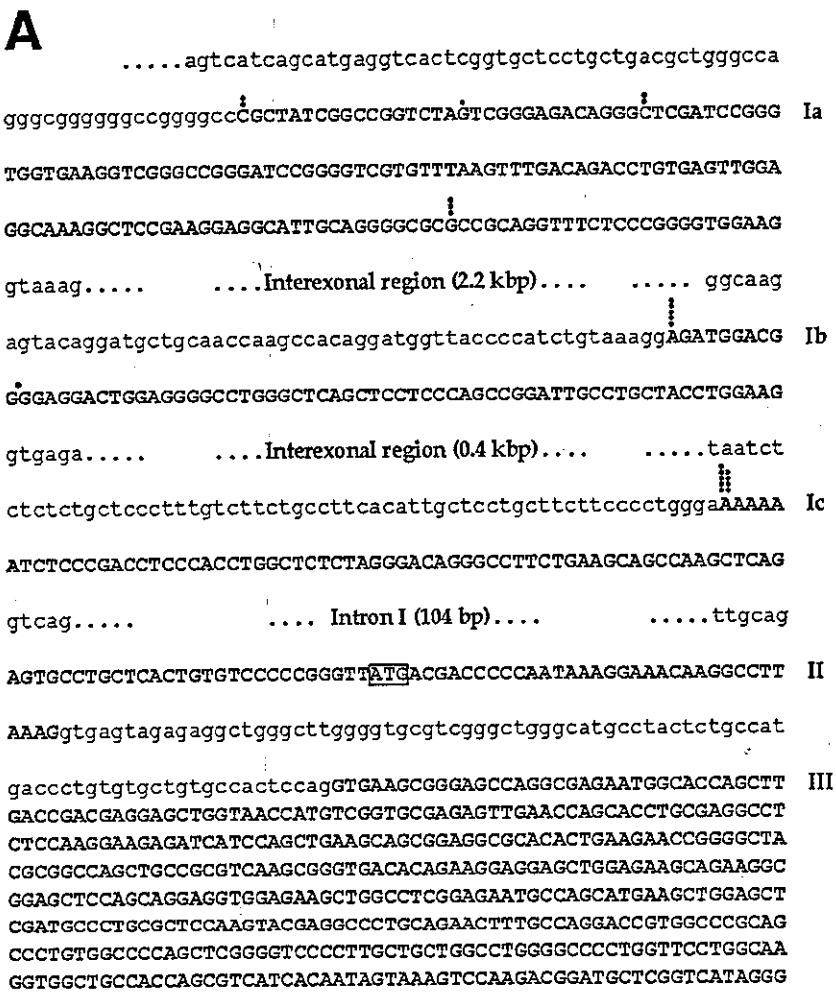

FIG. 2. **Multiple promoters are used for transcription of mouse *mafG*.** *A*, summary of 5′-RACE analysis. The sequences in *boldface, capital letters* represent exons, and those in *lowercase letters* represent introns or interexonal regions. The 5′-ends of the RACE clones are indicated by *solid circles*. The translational initiation ATG codon of *mafG* is *boxed*. *B*, structure of the mouse *mafG* gene and the four MafG mRNA splice isoforms identified by RACE. *C*, tissue distribution of the four MafG mRNA splice isoforms. cDNAs were synthesized from total RNAs prepared from the various tissues of adult animals, as indicated. The relative copy numbers of the MafG mRNA splice isoforms Ia, Ib, Ic, and Ic-int were determined by quantitative RT-PCR using a plasmid containing the cDNA for each splice isoform as the abundance standard. The relative copy number of the Ia splice isoform in brain was used as a reference and set to 1. The *error bars* represent the S.D. values (n = 3).

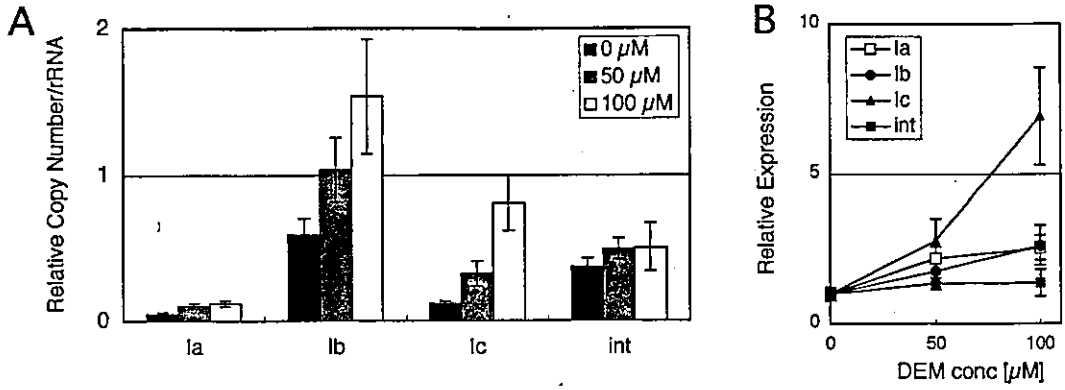

FIG. 3. **Inducibility of MafG splice isoforms by DEM.** *A* and *B*, quantitative RT-PCR was performed to examine the inducibility of the MafG mRNA splice isoforms Ia, Ib, Ic, and Ic-int by DEM. cDNAs were synthesized from total RNAs prepared from MEFs treated with 0, 50, and 100 μM DEM. The relative copy numbers of Ia, Ib, Ic, and Ic-int were quantified as described in the legend to Fig. 2. The *error bars* represent the S.D. values (n = 3). For *A*, the relative copy number of the Ia splice isoform with 0 μM of DEM was used as a reference and set to 1. For *B*, the relative copy number of each splice isoform with 0 μM DEM was used as a reference and set to 1.

dependent genes, induced the expression of *mafG* in MEF.[3] To confirm this observation, we treated wild type MEFs with DEM and examined the expression of small *maf* genes by quantitative RT-PCR. Among the small *maf* genes, *mafG* was the most significantly induced by DEM (Fig. 1*A*). Induction of *mafG* peaked 3 h after DEM treatment before gradually decreasing (Fig. 1*B*). Thus, *mafG* is a DEM-responsive gene induced at a relatively early stage in the course of the response. The *HO-1* gene showed a similar induction profile (Fig. 1*B*). Notably, the induction of other ARE-dependent genes, such as *NQO1* and *PRDX1*, peaked only after 12 h following DEM treatment (Fig. 1*B*).

The mafG Gene Has Three Alternative First Exons—To decipher the mechanisms controlling *mafG* induction, we examined transcriptional regulation of the *mafG* gene. We previously isolated phage clones containing the mouse *mafG* locus and mapped coding exons II and III but did not determine the nature of the noncoding first exon(s) (13). Therefore, we first performed 5′-RACE to determine first exon(s) utilized by the *mafG* gene and identified three (designated Ia, Ib, and Ic) (Fig. 2*A*). We also identified one splice isoform, designated "Ic-int" (Fig. 2*B*), which has an Ic first exon and intron sequence lying between the Ic and second exon but lacks the intron between exons II and III, demonstrating that this sequence was not due to genomic DNA contamination. We asked whether these splice isoforms (Ia, Ib, Ic, and Ic-int) are also found in the adult mouse and whether or not they are differentially utilized. To address the latter question, we designed a quantitative RT-PCR assay system which allowed specific transcript identification. Furthermore, to compare the relative abundance of each isoform, we prepared plasmid vectors containing each PCR product and used them as a copy number standard for quantitative RT-PCR. These results show that each splice isoform is differentially utilized (Fig. 2*C*). In the tissues tested, the Ib and Ic isoforms were relatively abundant (Fig. 2*C*). Whereas the Ia isoform was used relatively more rarely, this transcript seems to be preferentially expressed in hematopoietic tissues, such as spleen and bone marrow (Fig. 2*C*). The expression of the Ic-int isoform was utilized differently than the Ic isoform (Fig. 2*C*). In conclusion, accumulation of the four distinct MafG transcripts differs in a manner that is dependent on tissue type, suggesting that alternative transcriptional regulatory mechanisms differentially control expression from each of the three *mafG* promoters.

An ARE Consensus Sequence in the Promoter-proximal Region of mafG Exon Ic—We next asked whether the distinct *mafG* transcripts are utilized differentially in response to stress. We performed quantitative RT-PCR using cDNA recovered from cells treated or untreated with DEM. The Ia, Ib, and Ic isoforms were all significantly induced by DEM, whereas the Ic-int isoform was not (Fig. 3*A*). After DEM treatment, the Ib isoform was still the most abundant species of the *mafG* transcripts (Fig. 3*A*). Notably, upon comparison of the induction ratios for each transcript, we found that isoform Ic was most markedly induced (Fig. 3*B*).

While searching through the *mafG* genomic locus *in silico*, we discovered a potential ARE sequence 5′ to exon Ic (Ic-ARE) (Fig. 4*A*). The Ic-ARE partially matches the ideal ARE consensus sequence and is similar to the ARE identified in the NQO1 regulatory element (Fig. 4*A*). An NCBI data base search led to the identification of a putative first exon for human *mafG* corresponding nicely to the mouse Ic exon (Fig. 4*B*). The promoter-proximal region of exon Ic is highly conserved between mice and humans, including the putative *mafG* promoter Ic-ARE (Fig. 4*B*).

An Nrf2/MafG Heterodimer Binds to, and Activates Transcription from, the mafG Ic-ARE—The potential binding interaction of the Nrf2/small Maf heterodimer to the Ic-ARE was examined by EMSA. To assess the binding affinity of the *mafG* Ic-ARE, we compared it with the high affinity ARE site identified in the mouse NQO1 gene as a positive control. The result clearly demonstrated that the Nrf2/MafG heterodimer binds well to the *mafG* promoter ARE (Fig. 5*A*). The binding affinity of the heterodimer for the Ic-ARE appeared to be somewhat weaker than for the NQO1-ARE (Fig. 5*A*); in contrast, MafG homodimers seemed to prefer the MafG-ARE over the NQO1-ARE (Fig. 5*A*). The binding activities to the MafG-ARE were competed efficiently by a 300-fold molar excess of unlabeled wild type MafG-ARE, but not by the mutant MafG-ARE, possessing mutated nucleotides at both ends of the TPA response element contained within the MafG-ARE (m1) (Fig. 5*B*). These results showed that DNA binding of Nrf2 and MafG depends on the integrity of the TPA response element core sequence of the MafG-ARE. To the contrary, these binding activities were eliminated by the addition of a 300-fold molar excess of the mutated MafG-ARE possessing a mutation in the sequence lying just outside of the short ARE consensus (m2). The mutated MafG-ARE possessing both of the mutations within a single ARE (m3) behaved in a similar way with m1 mutant oligonucleotides (Fig. 5*B*). Further study using a lower molar excess of competitors showed that m2-type MafG-ARE was almost comparable with the wild type MafG-ARE in the ability to suppress the Nrf2/MafG-shifted complexes (Fig. 5*C*). These results showed that the mutated nucleotides in m2-type MafG-ARE are not

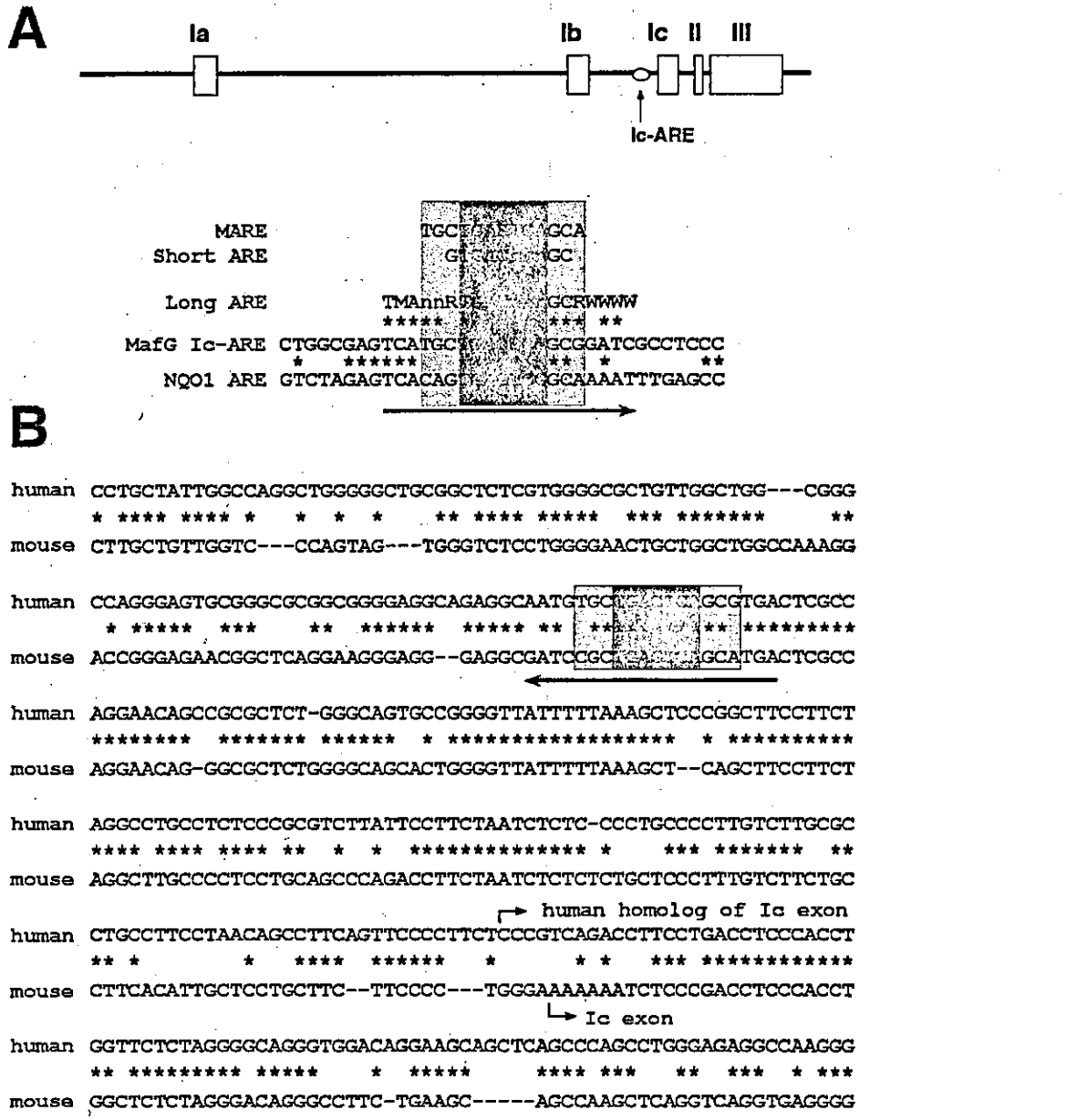

FIG. 4. **A putative ARE in the *mafG* gene Ic promoter.** *A*, alignment of the MARE, the short ARE, the long ARE, the mafG Ic-ARE, and the ARE from the mouse *NQO1* gene regulatory region. The MafG genomic locus is depicted at the *top*. The *boxes* represent exons, and the *circle* indicates the position of the *mafG* Ic-ARE. Each sequence was aligned, with *asterisks* indicating the nucleotides that are identical between the long ARE and the MafG Ic-ARE or between the MafG Ic-ARE and the NQO1 ARE. *B*, comparison of the first exons and the 5′ upstream regulatory regions of human and mouse *mafG* genes. For *A* and *B*, the *arrows* indicate nucleotides corresponding to the long ARE. The TPA response elopement core sequence of the MARE is *shaded* in *dark gray*. The GC boxes of the MARE are *shaded* in *light gray*. The abbreviations follow standard IUPAC nomenclature (where M represents A or C, R is A or G, Y is C or T, W is A or T, and S is G or C).

critical for the binding of Nrf2/MafG heterodimer and MafG homodimer to Ic-ARE at least *in vitro* (Fig. 5*C*).

To examine whether the *mafG* promoter Ic-ARE is functional, we performed transient transfection assays. Oligonucleotides containing ARE sequences were inserted into luciferase reporter genes and transfected into 293T cells. In order to make a comparison with the activity of a known ARE, we co-transfected luciferase reporter constructs containing either the ARE from *mafG* promoter or the ARE derived from the mouse *NQO1* gene. The ARE reporter gene was strongly activated by co-transfection with the Nrf2 expression vector alone (Fig. 5*D*). The ARE/luciferase reporter was activated to even higher levels when co-transfected with expression vectors that simultaneously forced Nrf2 and MafG expression (Fig. 5*D*). The induction of the reporter gene was comparable using either the *mafG* promoter or NQO1 promoter ARE sites (Fig. 5*D*). We further dissected the Ic-ARE activity by investigating the trans-activation potential of mutant AREs tested in EMSA. Strong induction of the reporter gene that is normally elicited by the Nrf2 expression vector was no longer observed with a mutated reporter gene possessing an m1-type mutation (Fig. 5*E*). Consistent with the result of EMSA, this showed that the TPA response element core sequence of the Ic-ARE is critical. Whereas m2-type mutation did not affect the binding activity of Nrf2/MafG, this mutation abolished Nrf2-mediated induction of the ARE luciferase reporter gene (Fig. 5*E*). It is noteworthy that both m1-type and m2-type mutated reporter genes were slightly activated when both Nrf2 and MafG expression vectors were co-introduced by transfection. However, no combination of factors was able to activate the reporter gene possessing the

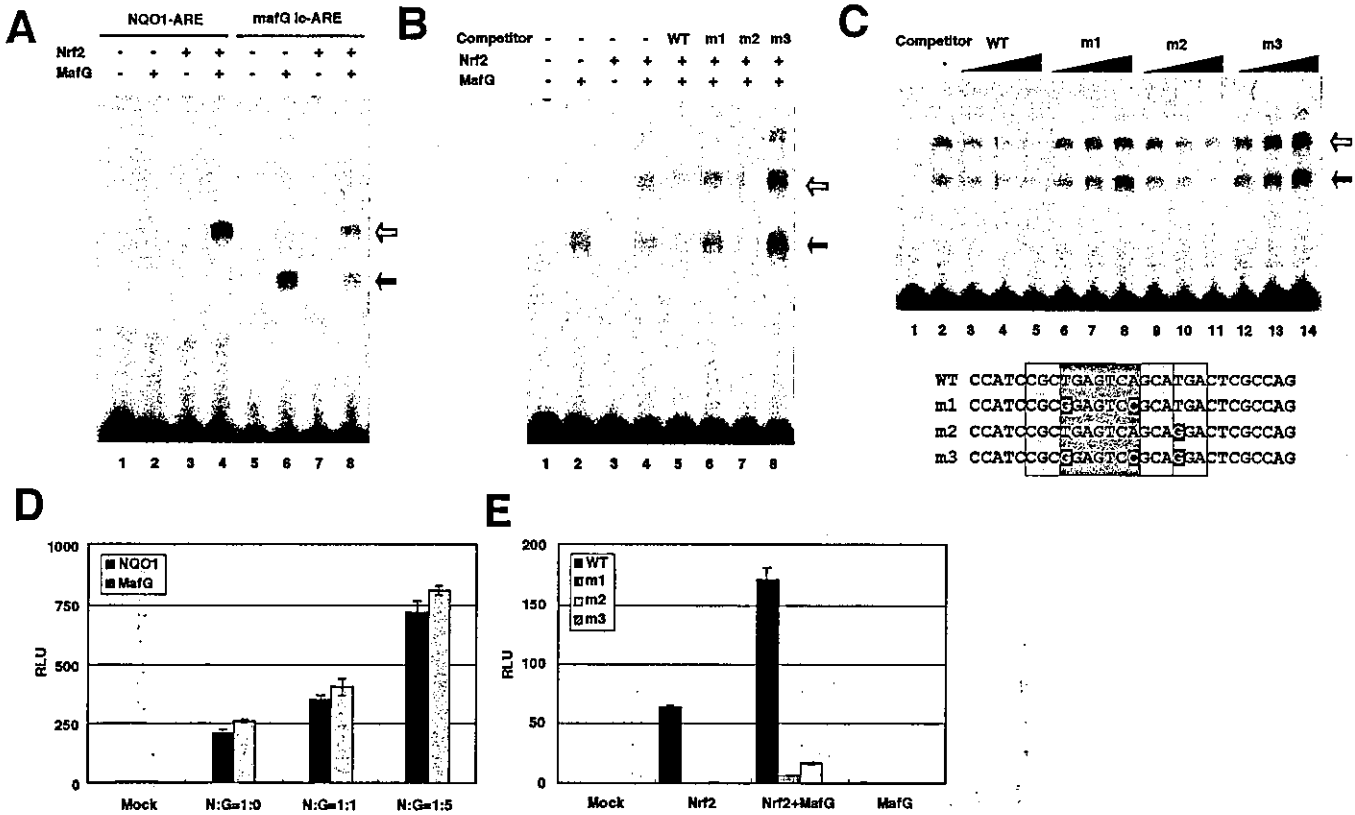

FIG. 5. **Nrf2 and MafG bind to the *mafG* promoter ARE, and cooperatively activate *mafG* transcription *in vitro*.** *A*, EMSA was performed with probes containing the *mafG* Ic-ARE or the ARE from the mouse *NQO1* gene regulatory region. Recombinant MafG and/or Nrf2 proteins were incubated with the probes, and the protein-DNA complexes and free probes were resolved by electrophoresis as described under "Experimental Procedures." No protein (*lanes 1* and *5*), MafG only (*lanes 2* and *6*), Nrf2 only (*lanes 3* and *7*), and both MafG and Nrf2 (*lanes 4* and *8*) were added to the reaction containing the probes. The *open arrow* indicates an Nrf2/MafG heterodimer complex, and the *closed arrow* indicates an MafG homodimer complex. *B*, Nrf2 and MafG proteins were incubated in combination in the absence (−) or presence (+) of a 300-fold molar excess of unlabeled competitor DNA. *Lanes 1–4* are in the same arrangement as *lanes 5–8* in *A*, respectively. Wild type (*WT*) competitor (*lane 5*) was unlabeled wild type *mafG* Ic-ARE. m1, m2, and m3 competitors (*lanes 6–8*) were unlabeled mutated *mafG* Ic-AREs. The mutated ARE sequences are shown in *C*. *C*, Nrf2 and MafG proteins were incubated in combination in the absence (−) or presence of a 10-fold (*lanes 3*, *6*, *9*, and *12*), 50-fold (*lanes 4*, *7*, *10*, and *13*), or 100-fold (*lanes 5*, *8*, *11*, and *14*) molar excess of unlabeled competitor DNA. Wild type (*lanes 2–5*), m1 (*lanes 6–8*), m2 (*lanes 9–11*), and m3 (*lanes 12–14*) competitors are used. *D*, 0.5 μg of pNQO1-ARE-luc and pMafG-ARE-luc reporter genes were transfected with various combinations of Nrf2 (*N*) and MafG (*G*) expression vectors into 293T cells. Except for the mock experiment, Nrf2 and MafG expression vectors were used in the following ratios: 1 (83 ng):0, 1:1, and 1:5. *E*, 500 ng of pNQO1-ARE-luc reporter gene and its ARE mutated derivatives were transfected with 83 ng of Nrf2 expression vector and/or 415 ng of MafG expression vector. The mutated ARE sequences are the same as used in EMSA shown in *C*. For *D* and *E*, firefly luciferase activity in the absence of any effector plasmid was set to 1 as the relative luciferase unit (*RLU*). The *error bars* represent S.D. values ($n = 3$).

m3-type mutation (Fig. 5*E*). These mutational analyses suggest that the sequences outside of the classical short ARE are important for maximum induction of *mafG* transcription.

Nrf2 and Small Maf Interact with the Endogenous mafG Ic-ARE—In order to confirm the biological significance of the data obtained from both EMSA and reporter transfections, ChIP experiments were performed using Hepa-1c1c7 cells. To induce nuclear accumulation of Nrf2, Hepa-1c1c7 cells were treated with DEM for 3 h, fixed with formaldehyde, and used for ChIP assays.

The association of Nrf2 with the NQO1 ARE was first examined as a positive control (22). As reported, Nrf2 and small Mafs associate strongly with the NQO1 ARE in DEM-treated cells but only weakly in mock-treated cells (Fig. 6). In the absence of IgG or in the presence of preimmune rabbit IgG, immunoprecipitations failed to select the NQO1 ARE (as well as other nonspecific genomic regions), demonstrating that the sites were not enriched in nonspecific fashion (Fig. 6). The *LDH* gene promoter region was not immunoprecipitated with either Nrf2 or small Mafs, suggesting that the antibodies used enriched DNA in a sequence-specific manner (Fig. 6). Under such conditions, these experiments showed that both Nrf2 and small Mafs associated with the *mafG* Ic-ARE in DEM-treated cells (Fig. 6). These results clearly

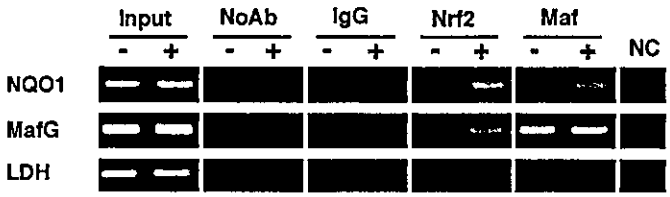

FIG. 6. **Nrf2 and MafK bind to the *mafG* Ic-ARE in an endogenous chromosomal context.** Hepa-1c1c7 cells were treated with DEM (+) or vehicle (−) for 3 h. Cross-linked nuclei were lysed and sonicated, and immunoprecipitations were performed using no antibody (*No Ab*), control rabbit IgG (*IgG*), anti-Nrf2 (*Nrf2*), or anti-small Maf (*Maf*). A portion of material not subjected to immunoprecipitation was used as a control (*Input*). *NC*, the PCR negative control. PCRs were performed using primers specific for the NQO1 regulatory region encompassing the ARE (*NQO1*), the MafG regulatory region encompassing the Ic-ARE (*MafG*), or the LDH promoter region (*LDH*).

demonstrated that Nrf2 and small Mafs can associate with an endogenous genomic region containing the *mafG* promoter Ic-ARE. Interestingly, small Mafs also strongly associated with the *mafG* Ic-ARE in vehicle-treated cells, suggesting occupation of the Ic-ARE by either inactive or repressive binding complexes prior to DEM induction.

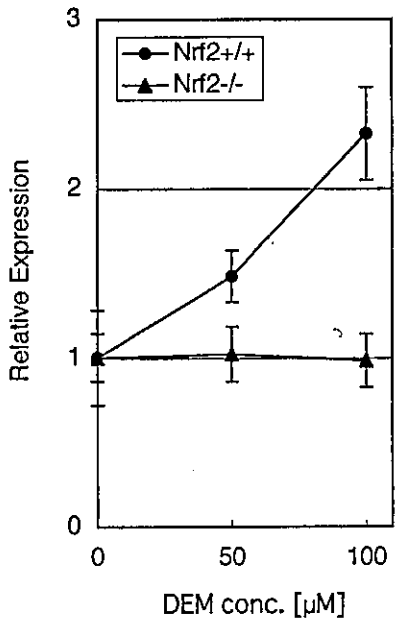

FIG. 7. ***MafG* induction is abolished in *nrf2*-null mutant fibroblasts.** MEFs were prepared from wild type and *nrf2*-null mutant mice and treated with 0, 50, and 100 μM DEM for 24 h. Total RNA was isolated from the cells and processed for quantitative RT-PCR. The expression of *mafG* with 0 μM DEM was set to 1. The *error bars* represent S.D. values (n = 3).

Induction of the mafG Gene Is Dependent on Nrf2—Finally, we sought genetic confirmation to support the dependence of *mafG* transcription on Nrf2 expression. To this end, we prepared *nrf2*-null embryonic fibroblasts, treated the cells with DEM, and examined *mafG* mRNA accumulation. Before DEM treatment, the expression of *mafG* was slightly elevated in *nrf2*-null mutant cells (in comparison with wild type controls) by ~1.5-fold. However, *mafG* was no longer significantly activated in *nrf2*-null mutant cells after adding DEM, whereas a dose-dependent induction of the *mafG* was observed in wild type cells (Fig. 7). These results demonstrate that *mafG* induction is dependent on Nrf2.

DISCUSSION

In this study, we examined the transcriptional regulation of the mouse *mafG* gene and concluded that *mafG* is itself an ARE-dependent gene controlled by Nrf2. In agreement with the present data, other Nrf2 inducers have also been reported to induce the *mafG* gene. A hamster *mafG* homolog was identified as a hydrogen peroxide-inducible gene in a differential display analysis of gene expression (23). Another group reported that pyrrolidine dithiocarbamate, a thiol compound, induces human *MAFG* (24). Furthermore, it has been reported that the zebrafish *mafG* homolog is inducible by DEM (25). Thus, *mafG* seems to be a stress-inducible gene in many species.

When we initially cloned the first exons of *mafG* by 5′-RACE analysis, we found that the mouse *mafG* gene has at least three alternative first exons (Ia, Ib, and Ic). We previously reported that *mafK* and *mafF* also have multiple untranslated first exons (14, 26). Taken together, it seems clear that all three small *maf* genes utilize multiple first exons. *MafG* does not appear to have tissue-specific first exons, such as the *mafK* I_N exon that is employed exclusively in neurons (27). Nonetheless, expression analysis revealed that *mafG* first exons are utilized differentially in various tissues.

Based on the sequences derived from the 5′-RACE clones, we concluded that none of the alternative splice isoforms of *mafG* produce a change in the amino acid composition of the protein. We inferred that utilizing multiple first exons presents itself as a solution by which small *maf* genes can confer distinct, broad (but not ubiquitous) expression profiles. Although we cloned a splice isoform of *mafG* (Ic-int) that contains the intron between exon Ic and exon II and is expressed at a significant level, its biological significance is yet to be determined.

All three first exons of *mafG* were induced upon oxidative stress. Whereas the Ib transcript was the most abundant before and after DEM treatment, the Ic transcript was the most strongly activated by DEM relative to its constitutive expression level. These observations show that the alternative first promoters vary in their inducible response to DEM. The critical transcription factor-binding site that could be responsible for DEM-mediated induction was anticipated to be an ARE(s). We searched for AREs in the *mafG* locus and identified one in the proximal promoter of exon Ic. Although the short ARE consensus sequence was originally defined as 5′-RGTGACnnnGC-3′, subsequent studies revealed that functional AREs, such as the one in the NQO1 gene, are often represented by a long ARE consensus sequence, 5′-TMAnnRTGAYnnnGCRwwww-3′ (22, 28). Indeed, the *mafG* Ic-ARE is similar to the longer consensus sequence and is also similar to the ARE found in the NQO1 gene regulatory region. Since the Ic-ARE is well conserved in the human *MAFG* gene, we suspect that these AREs are evolutionarily conserved for *mafG* regulation.

In at least two previous reports, investigators failed to observe cooperative activation of AREs by Nrf2 and small Maf proteins (29, 30). Although we also failed to observe this synergistic transcriptional activation in 3T3 or COS1 cells,[2] we did detect cooperativity in 293T cells. In the reporter analysis using 293T cells, we observed that the transcription mediated by the *mafG* Ic-ARE was cooperatively activated by Nrf2 and MafG. In this assay, a mutation outside the short ARE consensus of the Ic-ARE (Fig. 5*C*; m2) greatly inhibited induction of the reporter gene by Nrf2 and MafG. Since this mutation did not affect the binding of the Nrf2/Maf heterodimer in EMSA, unidentified factor(s), which recognize the sequence outside of ARE, might play critical cooperative roles with the Nrf2/Maf heterodimer in the transcriptional activation (31). Taken together, our observations provided support for the longer ARE consensus sequence as important for strong Nrf2-mediated induction.

ChIP analysis showed that Nrf2 actually binds to the *mafG* Ic-ARE in a chromosomal context. Moreover, DEM treatment of *nrf2*-null mutant cells led to no *mafG* induction. That is not to say that these data refute a possible contribution of Nrf1 or Nrf3 to *mafG* regulation, but in MEFs, neither Nrf1 nor Nrf3 is able to compensate for the absence of Nrf2. In fact, Nrf2 and Nrf1 have been shown to play important roles in ARE-dependent gene induction in an overlapping manner (8). ChIP analysis also showed that small Mafs bind to the *mafG* Ic-ARE. Although the small Maf antibody used in the ChIP assay recognizes primarily MafK, we suspect that all three small Maf proteins can bind to the *mafG* Ic-ARE, since this DNA binding motif is conserved among the small Maf proteins (5).

ChIP analysis showed that small Mafs bind to the *mafG* Ic-ARE even in untreated cells (Fig. 6), indicating that there is the small Maf binding activity independent of Nrf2. Since MafG homodimer is able to bind to the *mafG* Ic-ARE in EMSA, it is possible that small Maf proteins form inactive homodimers by themselves and occupy the *mafG* Ic-ARE in untreated cells. However, it is also possible that small Maf proteins heterodimerize with Bach1 to form a transcriptional repressor. The Bach1-MafG heterodimer may repress *mafG* gene transcription through *mafG* Ic-ARE in the same way as it represses *HO-1* gene expression (9, 16). The contribution of Bach1 proteins to the regulation of *mafG* is under investigation.

This study also showed that ARE-dependent genes are not induced uniformly by DEM. Indeed, *mafG* and *HO-1* were rapidly induced, whereas *NQO1* and *PRDX1* were slowly induced. These facts may help us to understand the biological significance of the induction of *mafG* upon exposure to oxidative stress. It is possible that rapidly induced genes may affect the expression of other ARE-dependent genes. Induced MafG could be utilized as a heterodimeric partner for Nrf2 to further induce ARE-dependent genes at a later stage of differentiation. On the other hand, induced MafG might heterodimerize with Bach1 or homodimerize with itself to repress ARE-dependent genes. These two possibilities are not mutually exclusive. We recently found that ARE-dependent genes are regulated differentially by small Maf proteins.[3] MafG induction may exert distinct influences on the expression levels of target genes, depending on their dimeric context.

Acknowledgments—We thank Dr Y. Kato for the Nrf2 expression plasmids and Dr. T. O'Connor, T. Yamamoto, and R. Kawai for help.

REFERENCES

1. Primiano, T., Sutter, T. R., and Kensler, T. W. (1997) *Adv. Pharmacol.* **38**, 293–328
2. Talalay, P., Dinkova-Kostova, A. T., and Holtzclaw, W. D. (2003) *Adv. Enzyme Regul.* **43**, 121–134
3. Kataoka, K., Igarashi, K., Itoh, K., Fujiwara, K. T., Noda, M., Yamamoto, M., and Nishizawa, M. (1995) *Mol. Cell. Biol.* **15**, 2180–2190
4. Motohashi, H., Shavit, J. A., Igarashi, K., Yamamoto, M., and Engel, J. D. (1997) *Nucleic Acids Res.* **25**, 2953–2959
5. Motohashi, H., O'Connor, T., Katsuoka, F., Engel, J. D., and Yamamoto, M. (2002) *Gene (Amst.)* **294**, 1–12
6. Itoh, K., Chiba, T., Takahashi, S., Ishii, T., Igarashi, K., Katoh, Y., Oyake, T., Hayashi, N., Satoh, K., Hatayama, I., Yamamoto, M., and Nabeshima, Y. (1997) *Biochem. Biophys. Res. Commun.* **236**, 313–322
7. Chen, L., Kwong, M., Lu, R., Ginzinger, D., Lee, C., Leung, L., and Chan, J. Y. (2003) *Mol. Cell. Biol.* **23**, 4673–4686
8. Leung, L., Kwong, M., Hou, S., Lee, C., and Chan, J. Y. (2003) *J. Biol. Chem.* **278**, 48021–48029
9. Sun, J., Hoshino, H., Takaku, K., Nakajima, O., Muto, A., Suzuki, H., Tashiro, S., Takahashi, S., Shibahara, S., Alam, J., Taketo, M. M., Yamamoto, M., and Igarashi, K. (2002) *EMBO J.* **21**, 5216–5224
10. Derjuga, A., Gourley, T. S., Holm, T. M., Heng, H. H., Shivdasani, R. A., Ahmed, R., Andrews, N. C., and Blank, V. (2004) *Mol. Cell. Biol.* **24**, 3286–3294
11. Muto, A., Tashiro, S., Nakajima, O., Hoshino, H., Takahashi, S., Sakoda, E., Ikebe, D., Yamamoto, M., and Igarashi, K. (2004) *Nature* **429**, 566–571
12. Kotkow, K. J., and Orkin, S. H. (1996) *Proc. Natl. Acad. Sci. U. S. A.* **93**, 3514–3518
13. Shavit, J. A., Motohashi, H., Onodera, K., Akasaka, J., Yamamoto, M., and Engel, J. D. (1998) *Genes Dev.* **12**, 2164–2174
14. Onodera, K., Shavit, J. A., Motohashi, H., Katsuoka, F., Akasaka, J. E., Engel, J. D., and Yamamoto, M. (1999) *J. Biol. Chem.* **274**, 21162–21169
15. Onodera, K., Shavit, J. A., Motohashi, H., Yamamoto, M., and Engel, J. D. (2000) *EMBO J.* **19**, 1335–1345
16. Katsuoka, F., Motohashi, H., Tamagawa, Y., Kure, S., Igarashi, K., Engel, J. D., and Yamamoto, M. (2003) *Mol. Cell. Biol.* **23**, 1163–1174
17. Ishii, T., Itoh, K., Takahashi, S., Sato, H., Yanagawa, T., Katoh, Y., Bannai, S., and Yamamoto, M. (2000) *J. Biol. Chem.* **275**, 16023–16029
18. Katoh, Y., Itoh, K., Yoshida, E., Miyagishi, M., Fukamizu, A., and Yamamoto, M. (2001) *Genes Cells* **6**, 857–868
19. Kyo, M., Yamamoto, T., Motohashi, H., Kamiya, T., Kuroita, T., Tanaka, T., Engel, J. D., Kawakami, B., and Yamamoto, M. (2004) *Genes Cells* **9**, 153–164
20. Motohashi, H., Katsuoka, F., Shavit, J. A., Engel, J. D., and Yamamoto, M. (2000) *Cell* **103**, 865–875
21. Igarashi, K., Itoh, K., Motohashi, H., Hayashi, N., Matuzaki, Y., Nakauchi, H., Nishizawa, M., and Yamamoto, M. (1995) *J. Biol. Chem.* **270**, 7615–7624
22. Nioi, P., McMahon, M., Itoh, K., Yamamoto, M., and Hayes, J. D. (2003) *Biochem. J.* **374**, 337–348
23. Crawford, D. R., Leahy, K. P., Wang, Y., Schools, G. P., Kochheiser, J. C., and Davies, K. J. (1996) *Free Radic. Biol. Med.* **21**, 521–525
24. Moran, J. A., Dahl, E. L., and Mulcahy, R. T. (2002) *Biochem. J.* **361**, 371–377
25. Takagi, Y., Kobayashi, M., Li, L., Suzuki, T., Nishikawa, K., and Yamamoto, M. (2004) *Biochem. Biophys. Res. Commun.* **320**, 62–69
26. Motohashi, H., Igarashi, K., Onodera, K., Takahashi, S., Ohtani, H., Nakafuku, M., Nishizawa, M., Engel, J. D., and Yamamoto, M. (1996) *Genes Cells* **1**, 223–238
27. Motohashi, H., Ohta, J., Engel, J. D., and Yamamoto, M. (1998) *Genes Cells* **3**, 671–684
28. Wasserman, W. W., and Fahl, W. E. (1997) *Proc. Natl. Acad. Sci. U. S. A.* **94**, 5361–5366
29. Dhakshinamoorthy, S., and Jaiswal, A. K. (2000) *J. Biol. Chem.* **275**, 40134–40141
30. Nguyen, T., Huang, H. C., and Pickett, C. B. (2000) *J. Biol. Chem.* **275**, 15466–15473
31. Wasserman, W. W., and Fahl, W. E. (1997) *Arch. Biochem. Biophys.* **344**, 387–396

Available online at www.sciencedirect.com
SCIENCE DIRECT®
Archives of Biochemistry and Biophysics 433 (2005) 342–350
ABB
www.elsevier.com/locate/yabbi

Evolutionary conserved N-terminal domain of Nrf2 is essential for the Keap1-mediated degradation of the protein by proteasome

Yasutake Katoh[a,b], Katsuyuki Iida[a], Moon-IL Kang[a], Akira Kobayashi[a], Mio Mizukami[b], Kit I. Tong[a], Michael McMahon[d], John D. Hayes[d], Ken Itoh[a,b], Masayuki Yamamoto[a,b,c,*]

[a] *Graduate School of Comprehensive Human Sciences, University of Tsukuba, 1-1-1 Tennoudai, Tsukuba 305-8577, Japan*
[b] *JST-ERATO Environmental Response Project, University of Tsukuba, 1-1-1 Tennoudai, Tsukuba 305-8577, Japan*
[c] *Center for Tsukuba Advanced Research Alliance, University of Tsukuba, 1-1-1 Tennoudai, Tsukuba 305-8577, Japan*
[d] *Biomedical Research Centre, Ninewells Hospital and Medical School, University of Dundee, Dundee DD1 9SY, Scotland, United Kingdom*

Received 13 September 2004, and in revised form 4 October 2004

Abstract

Under homeostatic conditions, Nrf2 activity is constitutively repressed. This process is dependent on Keap1, to which Nrf2 binds through the Neh2 domain. Since the N-terminal subdomain of Neh2 (Neh2-NT) contains evolutionarily conserved motifs, we examined the roles they play in the degradation of Nrf2. In Neh2-NT, we defined a novel motif that is distinct from the previously characterized DIDLID motif and designated it DLG motif. Deletion of Neh2-NT or mutation of the DLG motif largely abolished the Keap1-mediated degradation of Nrf2. These mutations were found to enfeeble the binding affinity of Nrf2 to Keap1. The Neh2-NT subdomain directed DLG-dependent, Keap1-independent, degradation of a reporter protein in the nucleus. By contrast, mutation of DLG did not affect the half-life of native Nrf2 protein in the nucleus under oxidative stress conditions. These results thus demonstrate that DLG motif plays essential roles in the Keap1-mediated proteasomal degradation of Nrf2 in the cytoplasm.

Keywords: Nrf2; Keap1; Degradation; Proteasome; Ubiquitination

Adaptive response to electrophilic or reactive oxygen species (ROS)[1] represents one of the most important cellular defense mechanisms against environmental toxins in animals [1,2]. Transcription factor Nrf2 (NF-E2-related factor 2) [3], also called ECH (erythroid-derived CNC homology protein) [4], that belongs to the Cap-N-Collar (CNC) family of transcription factors regulates the coordinated expression of a battery of cytoprotective genes under the regulation of electrophile responsive element/antioxidant responsive element (EpRE/ARE) enhancers [5,6]. Nrf2 requires a member of the small Maf proteins as an obligatory partner molecule for binding to its cognate DNA sequence [4,7]. The Nrf2/ARE regulated gene battery includes a subset of drug metabolizing enzymes, such as glutathione *S*-transferases (GSTs) [8] and NAD(P)H-quinone oxidoreductase 1 (NQO1) [9], and a subset of antioxidant genes, such as heme oxygenase-1 (HO-1) [10], the subunits of γ-glutamylcysteine synthetase (γ-GCS) [11], and thioredoxin [12]. *Nrf2*$^{-/-}$ mice deficient in this coordinated genetic program are susceptible to various oxidative stresses including acetaminophen intoxication [13,14], BHT intoxication [15], chemical carcinogenesis [16],

* Corresponding author. Fax: +81 298 53 7318.
E-mail address: masi@tara.tsukuba.ac.jp (M. Yamamoto).

[1] *Abbreviations used:* Nrf2, NF-E2-related factor 2; ROS, reactive oxygen species; ECH, erythroid-derived CNC homology protein; CNC, Cap-N-Collar; EpRE/ARE, electrophile responsive element/antioxidant responsive element; GSTs, glutathione *S*-transferases; NQO1; NAD(P)H-quinone oxidoreductase 1; HO-1, heme oxygenase-1; γ-GCS, γ-glutamylcysteine synthetase; Neh2-NT, N-terminal subdomain of Neh2.

0003-9861/$ - see front matter © 2004 Elsevier Inc. All rights reserved.
doi:10.1016/j.abb.2004.10.012

hyperoxia [17], and inhalation of diesel exhaust fumes [18].

Nrf2 activity is primarily repressed by Keap1-mediated sequestration of Nrf2 in cytosol [19,20]. Electrophiles modify highly reactive cysteines in Keap1 and inhibit its interaction with Nrf2 [21]. Accumulating lines of evidence demonstrated that Nrf2 activity is also downregulated by the proteasome [22–26]. Treatment of cells with electrophiles significantly prolonged the half-life of Nrf2. The N-terminal Neh2 domain of Nrf2 (amino acid residues 1–95) interacts with Keap1 in a redox-dependent fashion to allow its rapid degradation under homeostatic non-stressed conditions [25,26]. Based mainly on the analysis of *Keap1* knockout mice, we distinguished two modes of Nrf2 degradation: one mechanism is a Keap1-dependent proteasomal degradation that occurs under homeostatic conditions, and the other is a Keap1-independent Nrf2 degradation that occurs in the nucleus under oxidative stress conditions [25,26]. Using transient co-transfection experiments, it has been shown that Keap1 enhances Neh2-dependent degradation of Nrf2 in COS1 cells under homeostatic conditions [26]. Furthermore, the same study revealed that Nrf2 is constitutively ubiquitinated in a Keap1- and redox-independent manner, suggesting that Keap1 enhances Nrf2 degradation by post-ubiquitination mechanism in this cell line. By contrast with these findings, Zhang and Hannink [27] recently demonstrated that Keap1 enhances Nrf2 ubiquitination in MDA-MB-231 breast cancer cell line [27]. They also demonstrated that two cysteines C^{273} and C^{288} of Keap1 are indispensable for Keap1-mediated ubiquitination of Nrf2. On the other hand, Kobayashi et al. [28] recently demonstrated that Keap1 functions as an adaptor for Cul3-based E3 ligase to regulate proteasomal degradation of Nrf2.

To further explore the degradation mechanism of Nrf2, in this study, we focused on the role of N-terminal region of Neh2 (Neh2-NT) in Nrf2 degradation. We found that Neh2-NT mediates the Keap1-independent proteasomal degradation of EGFP in the nucleus when fused as a chimeric protein. A cluster of leucine residues in a putative α-helix within Neh2-NT was found to be essential for protein degradation in the nucleus. However, mutation of these leucine residues in native Nrf2 only marginally affected its half-life in the nucleus during conditions of oxidative stress. Conversely, these leucine residues were essential for the Keap1-mediated proteasomal degradation of native Nrf2 under normal homeostatic conditions. Unexpectedly, mutations introduced into Neh2-NT markedly decreased the binding affinity of Nrf2 to Keap1. Our results thus demonstrate that the newly identified amino acid conservation in Neh2 that is referred to as the DLG motif is required, along with the previously identified ETGE motif, for effective Keap1-mediated proteasomal degradation of Nrf2.

Materials and methods

Plasmid construction

To generate mammalian expression plasmids for mouse Neh2-EGFP and its derivatives, cDNA fragments containing wild-type Neh2 (1–99 amino acids (a.a.)), N-terminal Neh2 (Neh2-NT; 1–43 a.a.), C-terminal Neh2 (Neh2-CT; 44–99 a.a.), and Neh2-NT cDNA with three leucine to alanine substitutions (Neh2-LA) were cloned individually into the *Kpn*I site of pcDNA3/EGFP that was described in [29]. Expression plasmids for Nrf2-ΔNeh2-NT, and Nrf2-LA were generated by replacing cDNA fragment with mutations with that of wild-type Nrf2 [30].

Cell culture

NIH3T3, Cos7, 293T, and QT6 cells were maintained in Dulbecco's modified Eagle's medium (DMEM) supplemented with 10% fetal bovine serum (FBS). To generate stable transformants, NIH3T3 cells were transfected with 20 μg of Neh2-EGFP or EGFP expression plasmid by the calcium phosphate precipitation method [31] and subsequently cultured in DMEM containing 500-μg/ml G418 for 1 month.

The half-lives determination

The NIH3T3 cells were treated with 10-μM MG132 (PEPTIDE INSTITUTE) for 12 h. To remove MG132 from the culture, the cells were washed three times with phosphate buffered saline (PBS) and the cells were subsequently incubated with 20-μg/ml cycloheximide (CHX). Cos7 cells were incubated with 50-μg/ml CHX. Band intensities were measured by densitometric analysis and intensities of Western blot bands were plotted on a semi-logarithmic chart.

Immunoblotting

NIH3T3 cells were centrifuged and solubilized in 50-μl cell lysis buffer (10 mM Tris–HCl (pH 7.5), 1.5 mM $MgCl_2$, 150 mM NaCl, 0.5% NP-40, 1 mM PMSF, 3 mM DTT, and 1× Complete tablet (Roche)). Cell lysates were incubated on ice for 2 min and centrifuged at 10,000*g* for 15 min. Cos7 cells were directly solubilized with SDS sample buffer. Aliquots, 25-μg protein of NIH3T3 cell lysate or 30-μg protein of Cos7 cell lysate, were separated by SDS–polyacrylamide gel electrophoresis in the presence of 2-mercaptoethanol. The proteins were subsequently electro-transferred onto Immobilon membrane (Millipore). The blot was then probed by polyclonal rabbit antiserum against GFP (Santa Cruz Biotechnology), followed by horseradish peroxidase-conjugated anti-rabbit IgG. Signals were detected using ECL Plus Western blotting reagent (Amersham, Japan).

Immunoprecipitation

To determine the interaction of Keap1 with Nrf2 in cell culture, 293T cells were transfected with an Nrf2 expression plasmid along with a HA-tagged Keap1 expression plasmid, and an immunoprecipitation experiment was performed. Whole cell extracts of 293T cells were prepared in RIPA buffer (10 mM Tris–HCl (pH 7.5), 150 mM NaCl, 1 mM EDTA, 0.1% deoxycholate, 0.1% SDS, 1% Nonidet P-40, and protease inhibitor cocktail (Roche Diagnostic)), and mixed for 3 h at 4 °C with an anti-Keap1 antibody against the N-terminal portion of the protein. Immuno-complexes were precipitated with Protein G (Pierce), washed three times with lysis buffer, and subjected to immunoblot analysis by anti-Keap1 antibody or anti-Nrf2 antibody.

Luciferase assay

QT6 and 293T cells were transfected using calcium phosphate precipitation as previously described [31]. The luciferase assay was performed by utilizing the Dual-Luciferase Reporter Assay System (Promega, Madison, WI) following the supplier's protocol and measured in a Biolumat Luminometer (Berthold, Germany). Transfection efficiencies were routinely normalized to the activity of a co-transfected *Renilla* luciferase expression plasmid, pRL-TK. Three independent experiments, each carried out in duplicate, were performed.

Results

Keap1-independent degradation of Neh2-EGFP in the nucleus

To elucidate the degradation mechanisms of Nrf2, we first examined the contribution that the Neh2 domain makes to the degradation of Nrf2 in the nucleus. We previously reported that when Neh2-EGFP protein (Neh2 (1–99 a.a.) fused with EGFP) was stably transfected into NIH3T3 fibroblasts, it was degraded rapidly. As Neh2-EGFP mainly accumulated in the nucleus in our assay condition, we assumed that the degradation of Neh2-EGFP mainly occurred in the nucleus [25,29]. Consistent with this notion, Neh2-EGFP fused to nuclear localization signal (Neh2-NLS-EGFP) degraded with a half-life similar to that for the wild-type Neh2-EGFP (data not shown). These results argue that upon transfection into NIH3T3 fibroblasts Neh2-EGFP is primarily degraded in a Keap1-independent manner in the nucleus.

We then fused N-terminal (1–43 a.a.) and C-terminal (44–99 a.a.) regions of Neh2 independently to EGFP (Neh2-NT-EGFP and Neh2-CT-EGFP, respectively) within a plasmid vector that harbors neomycin-resistance gene and transfected these constructs into NIH3T3 cells (Fig. 1A). Neomycin-resistant cells were selected with G418 and multiple mass stable transformants were established for each construct. Transformed cells were then treated with MG132 for 12 h to allow accumulation of fusion proteins. After thorough washing of the cells, the degradation half-lives of these EGFP fusion proteins were determined in the presence of the protein synthesis inhibitor cycloheximide (CHX). Immunoblot analysis with anti-EGFP antibody and subsequent densitometric analysis revealed that level of Neh2-NT-EGFP protein declined rapidly after the addition of CHX with a degradation half-life of 4 h, which is comparable to that for Neh2-EGFP protein. In contrast, Neh2-CT-EGFP remained stable over 8 h (Fig. 1B). These results thus indicate that the Neh2-NT region mediates the degradation of Nrf2 in the nucleus.

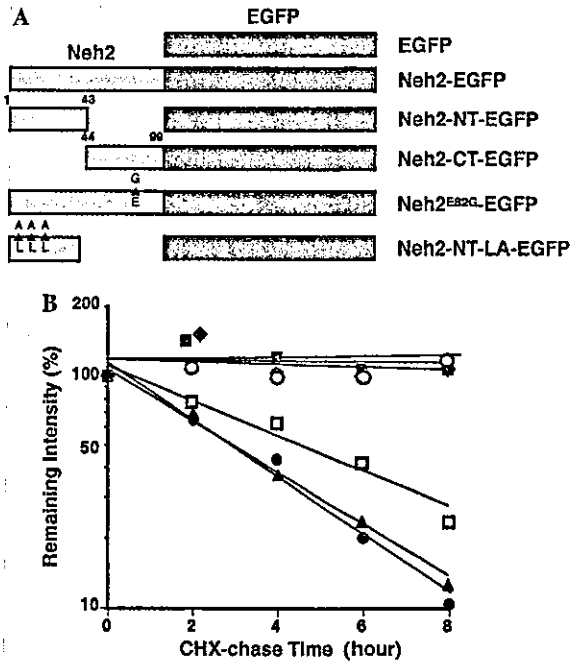

	$T_{1/2}$ (hr)		$T_{1/2}$ (hr)
EGFP	> 8.0	Neh2-CT-EGFP	> 8.0
Neh2-EGFP	2.4 ± 0.53	Neh2-NT-EGFP	3.3 ± 0.45
Neh2E82G-EGFP	2.5 ± 0.05	Neh2-NT-LA-EGFP	> 8.0

Fig. 1. Neh2-NT mediates proteasomal Nrf2 degradation in the nucleus in a DLG sequence-dependent manner. (A) Schematic representation of Neh2-EGFP fusion proteins. (B) Determination of protein half-lives of EGFP fusion proteins. Each EGFP fused protein was first accumulated by 10 μM MG132 for 12 h. The protein levels of EGFP, Neh2-EGFP, Neh2-NT-EGFP, Neh2-CT-EGFP, Neh2^{E82G} GFP, and Neh2-NT-LA-EGFP were determined using anti-EGFP antibody after treating the cells with 20 μg/ml CHX for indicated times. The relative intensity of EGFP against CHX-chase time (EGFP/β-actin) is shown in a semi-logarithmic plot and the calculated half-lives from three independent experiments are shown with SEM below the plot.

Neh2-NT is differentially conserved in CNC factors

We noticed that the N-terminal region of Neh2 is conserved widely in a group of CNC factors (Fig. 2A), including Nrf1, Nrf2, CncC, and SKN-1 [29,32,33]. We refer to this region (i.e., 1–43 a.a.) as the Neh2-NT subdomain in this paper. Upon detailed sequence comparison, we identified two motifs in the Neh2-NT subdomain that are conserved differentially among the CNC factors. One motif relates to the previously identified DIDLID element, which is conserved in Nrf1, Nrf2, and SKN-1, but not in CncC (Fig. 2B). The other motif corresponds to a specific sequence LxxQDxDLG, which is extensively conserved in the CNC factors. One important feature of the latter motif is that the motif is almost invariably linked to the presence of ETGE motif, which we previously identified as the motif essential for the interaction of Nrf2 with Keap1. Considering the tight linkage between the LxxQDxDLG sequence and the ETGE motif, we decided to analyze the contribution of the former sequence to the degradation of Nrf2. The LxxQDxDLG sequence will be referred to henceforth as the DLG motif after the C-terminal part (shaded in Fig. 2A).

The concomitant occurrence of the DLG and ETGE motifs suggests that the former may contribute to the interaction of Nrf2 with Keap1. Analysis of Neh2 secondary structure by Chou–Fasman algorithm predicts that the Neh2-NT subdomain adopts an α-helical struc-

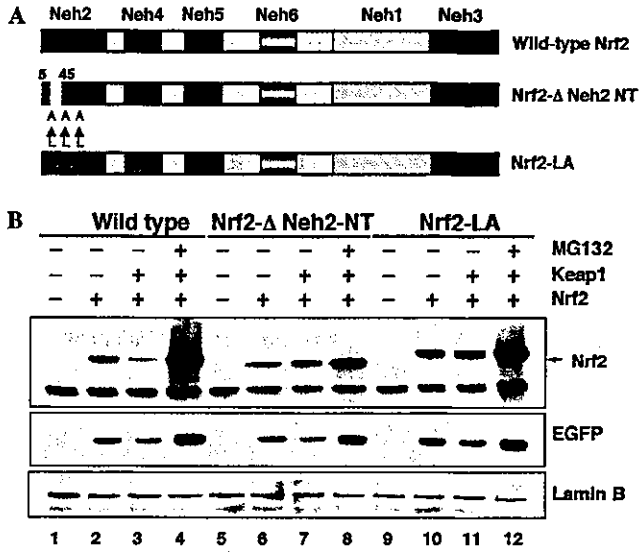

Fig. 3. Neh2-NT and leucine residues in the predicted α-helix are essential for Keap1-mediated degradation of Nrf2. (A) Schematic structure of Nrf2 mutant proteins. (B) Cos7 cells were transiently transfected with wild-type Nrf2 (lanes 1–4), Nrf2-ΔNeh2-NT (lanes 5–8) or Nrf2-LA (lanes 9–12) with (lanes 3, 4, 7, 8, 11, and 12) or without (1, 2, 5, 6, 9, and 10) Keap1 plasmid. Cell were also transfected with EGFP expression plasmid (lanes 2–4, 6–8, and 10–12) to standardize transfection efficiency. Cells were treated with 2 μM MG132 for 12 h before cell harvest (lanes 4, 8, and 12). Subsequently, total cell lysates were subjected to immunoblot analysis by anti-Nrf2 antibody (top panel), anti-EGFP antibody (middle panel) or anti-lamin B antibody (bottom panel).

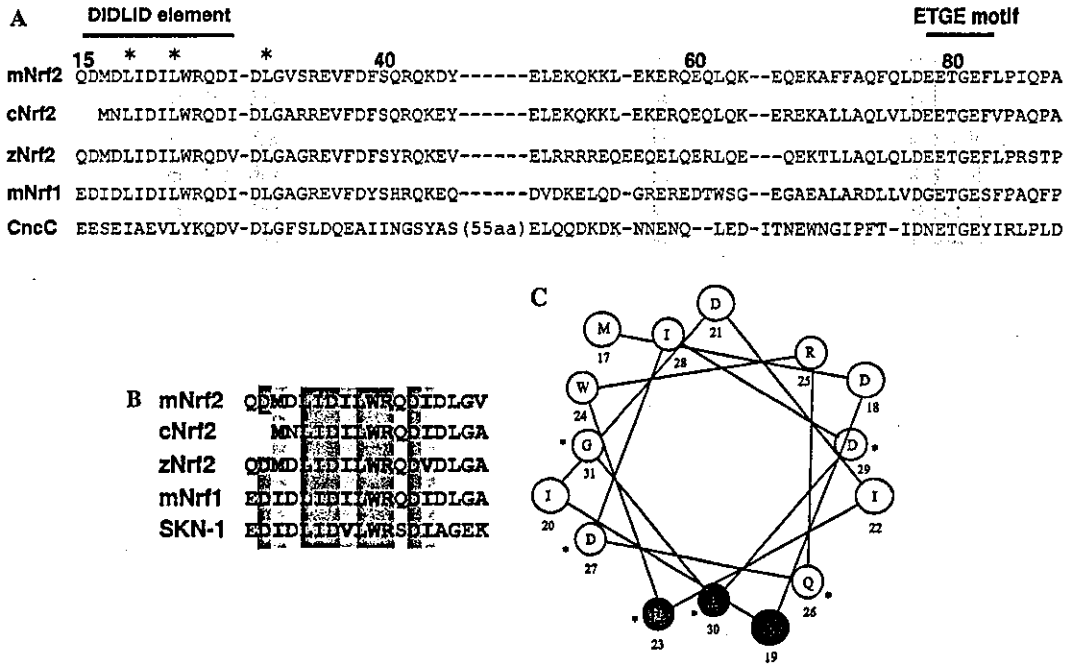

Fig. 2. Differential conservation of Neh2-NT region among CNC factors. (A) Sequence alignment of Neh2 region from CNC transcription factors. Amino acids conserved between Nrf2, Nrf1, and CncC are boxed with yellow color. (B) Amino acid conservation of previously identified DIDLID element. (C) Schematic representation of the predicted α-helix in Neh2-NT. Amino acids conserved between Nrf2, Nrf1, and CncC that are shaded in yellow in Fig. 2A are indicated by asterisks. A cluster of leucine residues is blanketed by red shades.